Bedrock incision and relief generation of the western Hangay Mountains, Mongolia

Tara Forstner
Department of Earth Sciences
Dalhousie University

Advisor
John Gosse
Department of Earth Sciences
Dalhousie University
Submitted in partial fulfillment of the requirements for the
Degree of Honours Bachelor of Science Earth Science
Dalhousie University

March 18, 2013

Distribution License

DalSpace requires agreement to this non-exclusive distribution license before your item can appear on DalSpace.

NON-EXCLUSIVE DISTRIBUTION LICENSE

You (the author(s) or copyright owner) grant to Dalhousie University the non-exclusive right to reproduce and distribute your submission worldwide in any medium.

You agree that Dalhousie University may, without changing the content, reformat the submission for the purpose of preservation.

You also agree that Dalhousie University may keep more than one copy of this submission for purposes of security, back-up and preservation.

You agree that the submission is your original work, and that you have the right to grant the rights contained in this license. You also agree that your submission does not, to the best of your knowledge, infringe upon anyone's copyright.

If the submission contains material for which you do not hold copyright, you agree that you have obtained the unrestricted permission of the copyright owner to grant Dalhousie University the rights required by this license, and that such third-party owned material is clearly identified and acknowledged within the text or content of the submission.

If the submission is based upon work that has been sponsored or supported by an agency or organization other than Dalhousie University, you assert that you have fulfilled any right of review or other obligations required by such contract or agreement.

Dalhousie University will clearly identify your name(s) as the author(s) or owner(s) of the submission, and will not make any alteration to the content of the files that you have submitted.

If you have questions regarding this license please contact the repository manager at dalspace@dal.ca.

Grant the distribution license by signing and dating below.

_____ _____

Name of signatory Date

DALHOUSIE UNIVERSITY
Inspiring Minds

Department of Earth Sciences
Halifax, Nova Scotia
Canada B3H 4R2
(902) 494-2358
FAX (902) 494-6889

DATE: April 26, 2013

AUTHOR: Tara Forstner

TITLE: Bedrock incision and relief generation of the western Hangay Mountains, Mongolia

Degree: Earth Sciences Convocation: May 23rd Year: 2013

Abstract

The origin of relief of the Hangay Mountains in west-central Mongolia is problematic because they are situated far from any plate boundary or major active tectonic structure. Straths, former stream bottoms preserved as bedrocks terraces, are useful indicators of rock uplift or foreland basin subsidence. By correlating and dating straths of differing heights preserved along valleys in the western Hangay Mountains, it is possible to relate this to the tectonic or isostatic processes that contribute to the relief.

Different methods were used to correlate 365 straths in 3 fourth-order stream valleys in western Hangay Mountains (Chigestei, Bogdiin, and Yaruu rivers). The straths were mapped in the field or identified from Google Earth®, and from slope- and surface-area-constrained querying of ASTER DEM data. No significant downstream convergence or divergence of the paleo-long profiles was apparent from either of the valleys. The strath distribution in all three valleys could be explained by slight divergence or convergence, although the strath correlations for the Yaruu valley favour slight a divergent pattern. The distribution of strath points on an elevation vs. valley distance plot for all three valleys is wider (more elevation) downstream, implying that all three valleys have undergone some divergence. The observation that the correlations and the distribution pattern do not record a steep convergence or divergence indicates that the basin or mountains are rising or falling together, and suggests that the incision has not been accelerated by rapid rock uplift of the upper catchment or rapid base level fall in the past few million years.

Cosmogenic ^{10}Be ages on strath terraces in the Chigestei and Bogdiin valleys were adjusted by an erosion rate (3.9 mm/yr) that is calculated by assuming that the highest ^{10}Be concentration is saturated and controlled by surface erosion. The ages range from 35.8±1 to 164±4 years. Because it is likely that the straths were eroded (geometry of the surfaces, lack of stream gravels on straths) and unlikely that the erosion rates were the same, these ages provide only estimates of the time they were abandoned. The calculated incision rates are very low (0 - 0.007 mm/yr). This slow incision rate supports the inference of slow incision based on the interpretation of strath patterns, and implies that there has not been significant relief generation in the past 0.3 Ma and probably over the last several million years.

Table of Contents

Table of Figures

Table of Tables

Chapter 1: Introduction

Landscapes with high elevation and low topography remain a first order problem in intracontinental dynamics, since vertical plate motion associated with epeirogenic uplift and subsidence is not well explained in the theory of plate tectonics. High continental plateaus with significant elevation but relatively low relief, are found in proximity to active tectonic margins (e.g. Puna-Altiplano Plateau in the convergent margin Andes, Tibetan Plateau adjacent to the collisional-margin Himalayas, Colorado Plateau adjacent to the basin and range province). Diffuse plate boundary deformational zones make it difficult to explain strong lateral variations of lithospheric structure (Wang et al., 2004). Precise estimates of plate motion have long been a major obstacle to quantify characterization of continental deformation (Thatcher, 2003).

The Hangay Mountains of western Mongolia are a large (~200 000 km^2) low-relief (<300 m) highland (>3000 m) embedded within the greater Mongolian Plateau (Fig. 1.1). It is situated at the northern extremity of diffuse-deformation from the far-field Indo-Eurasian plate collision and ~3000 km from the Japanese trench (Fig 1.1), the two nearest sources of collisional tectonics. The Mongolian Plateau is characterized as an extensive area that is several thousands of meters above the surrounding elevation. In this case, the Mongolia Plateau is ~1.2 km elevation above the Siberian Craton to the north which sits at an elevation ~350 m above sea level. Mountains, however, are regionally defined as high elevation peaks in an area defined as the range. The study of the Hangay Mountains will provide insight on the understanding of vertical movements associated with intracontinental tectonics, and the processes that

contribute to topography generation in high elevation landscapes away from collisional margins.

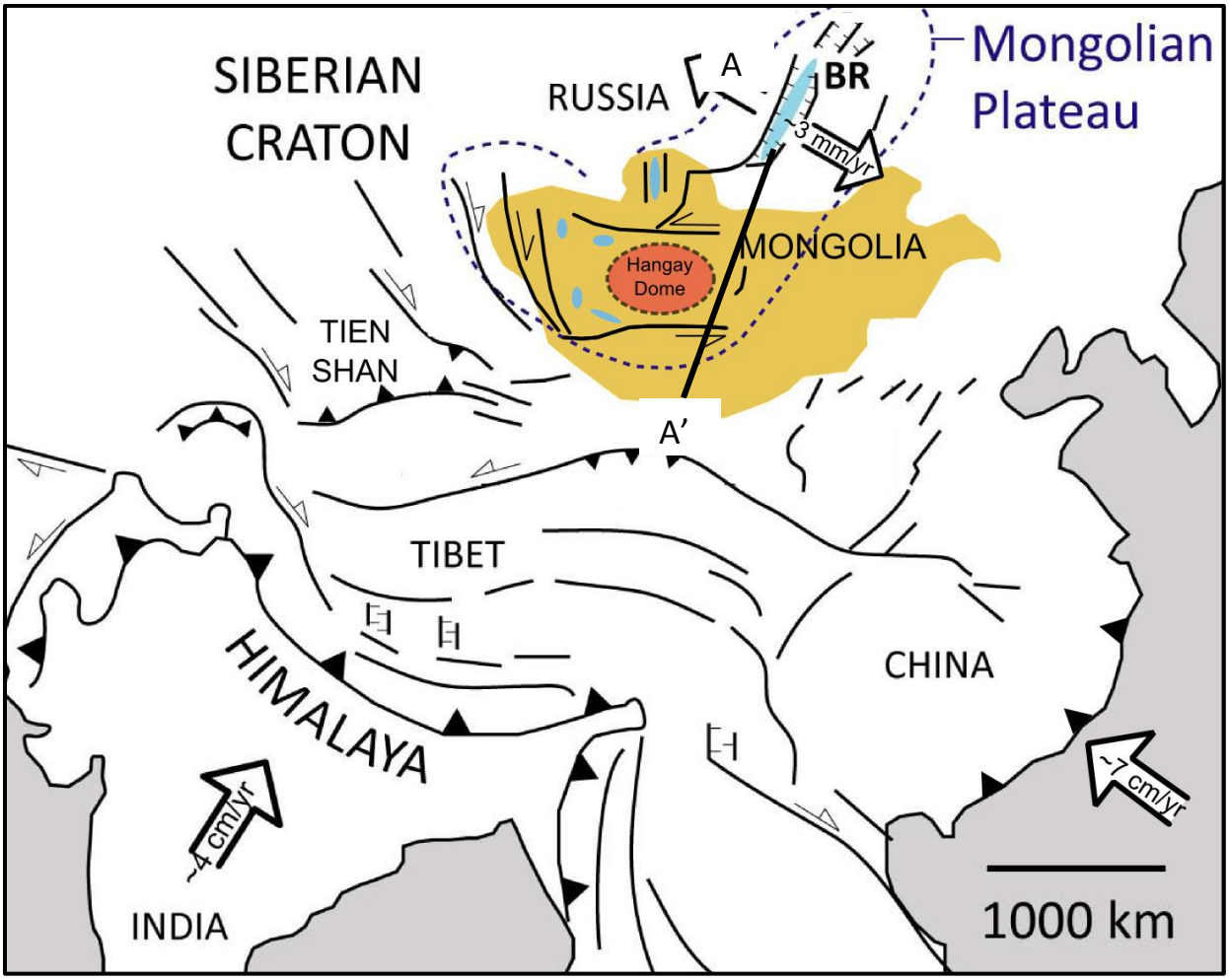

Fig 1.1. Simplified map of major faults and tectonics surrounding Mongolia. The Hangay Mountains are embedded within the larger Mongolian Plateau in central Mongolia. The India-Asian collision is ~2000 m to the south of the Hangay. The Siberian Craton borders the Mongolian boundary with Russia. The Baikal rift to the north is extending ~3 mm/yr. Map altered from Traynor and Sladen (1995).

The relief within the Hangay Mountains are mostly due to fluvial incision, although Pleistocene glaciation has contributed to the erosion of the higher elevations and individual Neogene fault scarps contribute metres of relief in places. The cause and timing of the surface

uplift leading to the mountain range is uncertain. Further, it is unclear if the current relief is associated with the surface uplift or a response to subsequent forcing.

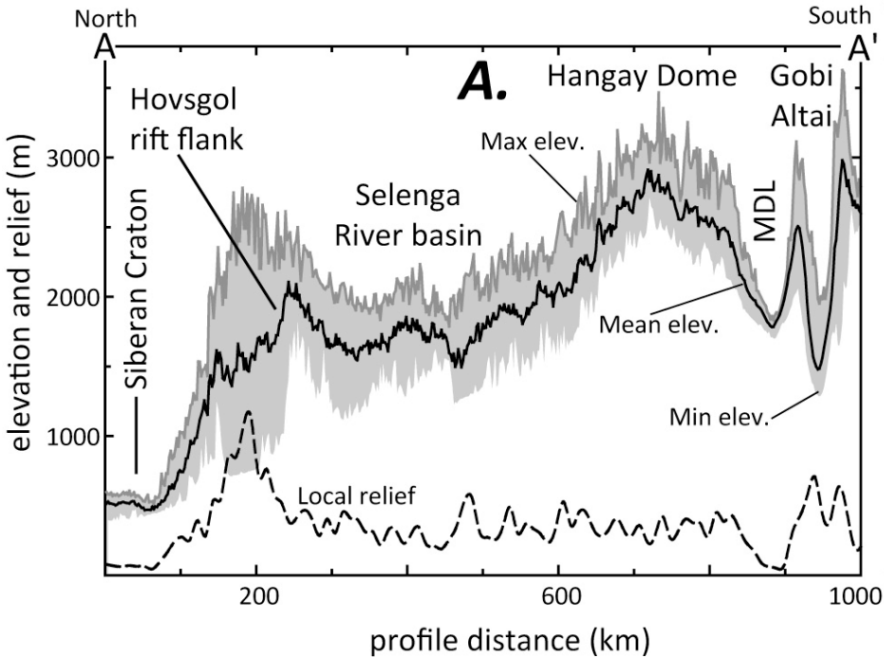

Fig 1.2. Topographic swath profile across Hangay Mountains derived from SRTM-90m data. Note high elevations compared to local relief. MDL - Mongolian Depression of Lakes (Jolivet et al., 2007).

H1. The regional topography of the Hangay Mountains is generated by surface uplift. The surface uplift may have been associated with rock uplift caused by far-field collisional tectonics (Cunningham, 2001) or mantle delamination (Barry et al., 2003). The alternative hypothesis is that the relief was generated by base level fall around the perimeter of the range. In this instance, the current relief is not related to rock uplift, but instead was generated as a response to a lowering of base level due to extensional tectonics adjacent to the mountain range.

To test H1, the history of stream incision will be used. The longitudinal profile of a stream is related to a number of factors including climate, catchment size, and rock characteristics (Merritts et al., 1994; Schumm, 1986). Stream gradients also respond to rock uplift or subsidence. If a stream incises to maintain equilibrium with these factors, it abandons previous stream bottoms above it. Stream bottoms of ancient streams are sometimes preserved along valley walls and can be recognized in the field and from remotely sensed imagery and used to map how the stream gradient has changed over time, for instance, if the headwaters are uplifting or the base level is dropping. If the surface has been uplifted, the stream incision will be greater in the headwaters that are rising, resulting in a down-stream convergence of paleo-longitudinal profiles for each valley affected by the uplift. Alternatively, if the basin controlling base-level has subsided, the paleo-longitudinal profiles will diverge downstream. The incision will then be greater in proximity to the basin, as the stream maintains an equilibrium gradient (Schumm, 1993).

Bedrock strath terraces representing abandoned paleo-long profiles of the Chigestei, Bogdiin, and Yaruu valleys, Western Hangay Mountains, were mapped to establish the trend with time. The results suggest that all three rivers show a slight downstream divergence, suggesting valley subsidence has continued over the duration recorded by the stream incision record. Minimum cosmogenic ^{10}Be exposure ages of the straths support the correlation and suggest slow rates of incision, and when adjusted for surface erosion, the ages become older and incision rates even slower.

Chapter 2: Background

Mongolia has three prominent mountain ranges, the Altai in the south, Hangay in central Mongolia, and the Khentii Mountains to the northeast of Ulaanbaatar. The Altai and Hangay Mountains trend northwest-southeast, but unlike the Altai Mountains, the Hangay Mountains are not bounded by north thrust faults from far-field deformation associated with the Indo-Eurasian collision. However, strike-slip and extensional fault systems are currently active in the south and north and western sections of the Hangay Mountains. The Hangay Mountains are the second highest range in Mongolia with the highest peak reaching 4000 m, and the basin relief is as high as 1000 m above the Valley of Great Lakes outlet on the west (Figure 2.1). Most drainages west of the Hangay drainage divide carry sediment to the internally drained Valley of Great Lakes to the southwest or through the expansive network to the northeast into Lake Baikal, Russia.

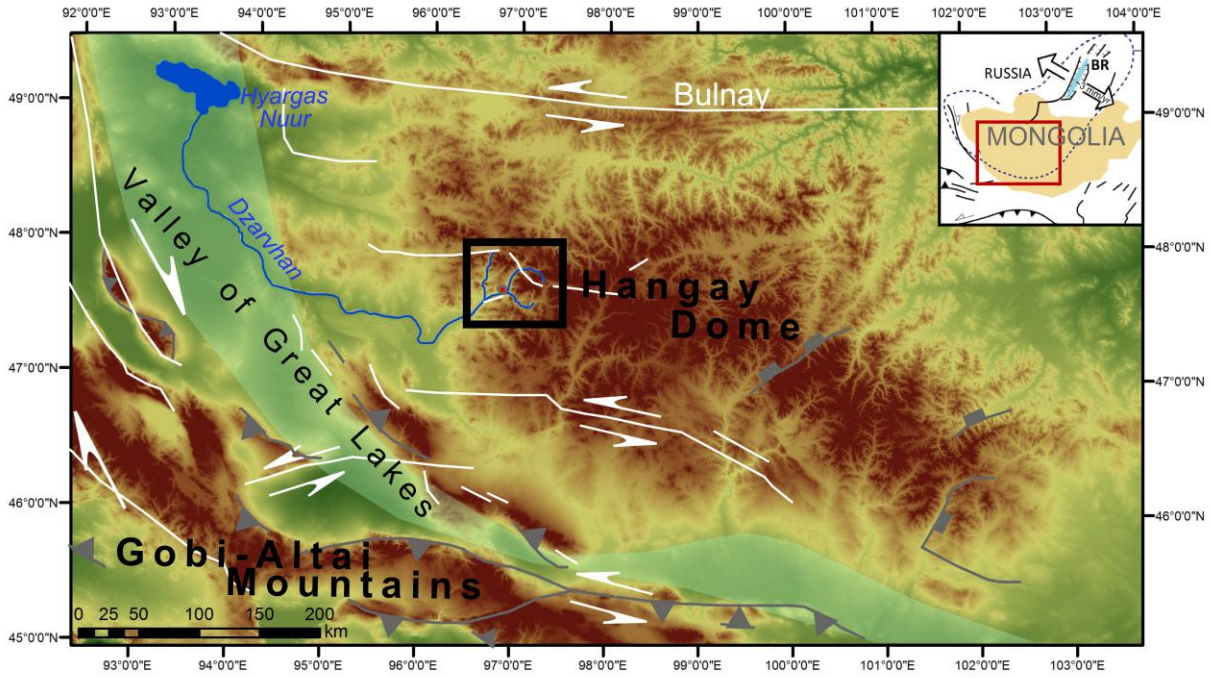

Fig. 2.1. Hangay Mountains and regional tectonics depicted on a 30-m DEM map based on ASTER data. The study area is the black box. The Dzarvhan river is shown draining into the Hyargas Lake which is in north-western Valley of Great Lakes. Strike slip faults are showed in white (Cunningham, 2001; Walker et al., 2008).

2.1. Setting

The Hangay Mountains are part of the Paleozoic Central Asian Orogenic Belt. Mongolian terranes are mostly composed of Precambrian mini-continents, cratonic blocks, Neoproterozoic to Early Paleozoic island arcs, back-arc basins, and ophiolitic suture complexes, all being accreted to the Siberian Craton in the Early Paleozoic (Donskaya et al., 2013). Late-Permian to Early Jurassic Khangai granitoids compose the structurally and spatially separated massifs of the Hangay Mountains (Yarmolyuk et al., 2008). Since the lithology of the mountain range is relatively uniform in the sense that there no sedimentary rocks in the studied drainages, incision rates are not strongly dependent on composition of the bedrock (Montgomery, 2004). Variations in fracture density and grain size do have local effects but these are smaller than the basin-scale analysis of this thesis.

Despite the limited recorded seismicity in the Hangay Mountains, the area is cut through by several left-lateral strike slip faults accommodating the regional shear between China and Siberia (Walker et al., 2008). This may suggest long recurrence intervals and large earthquakes. The Bulnay fault is a 375 km long east-west trending strike slip fault to the north of the Hangay Mountains. The 1905 rupture (M: 8.2-8.7) is one of the world's largest recorded intracontinental earthquakes (Rizza et al., 2009) and has an estimated slip rate of 4-16mm yr^{-1}. The left-lateral slip is accommodated in part by east-west extension across the Hovsgol graben system southwest of the Baikal rift (Baljinnyam, 1993). .

Based on the flux of sediment in the surrounding basins, it is estimated that Cenozoic shortening occurred mainly in the Oligocene (Devyatkin, 1974). However, the Hangay has a lack

of bounding thrusts with significant vertical component which suggests the relief of the range is not likely due to transpressional thrust faults (Cunningham, 2001).The Valley of Great Lakes are characterized as successor and compressional basins from normal reverse faults and transtensional strike-slip pull apart basins similar to the transpressional dynamics associated with the Altai thrust (Arzhannikova and Arzhannikov, 2008). The active extensional faulting could be a possible driving force of subsidence in the transpressional basins to the west of the mountains (Traynor and Sladen, 1995).

Our studies are focused on middle reaches of three streams in the headwaters of the Dzarvhan channel, which is a 410 km long drainage into Hyargas Nuur lake of the Valley of Great Lakes to the northwest of the Hangay (Figure 2.2). The Chigestei, Bogdiin, and Yaruu streams comprise the headwaters of the Dzarvhan, and are alluvial streams with varying floodplains of ~1500-300 m wide. The upper reaches of the Bogdiin stream show clear evidence of glaciation. The middle reaches are mostly restricted to steep-walled valleys containing strath and fill terrace fragments. Farther down valley, the Dzarvhan is a wide (1 km) river with no apparent floodplain before it drains into the Valley of Great Lakes. Many of the lakes in the Valley of Great Lakes have visible paleo-lake indicators such as raised beach ridges. Hyargas Nuur reached its maximum height of ~115 m above modern lake level during the late Pleistocene glaciations when there was a humid cold climate in the region (Arzhannikov and Arzhannikova, 2011). While this is a significant change in base level over a relatively short time (millennia to tens of millennia), because the gradient of the streams are relatively steep, the effect of this potentially cyclic base-level change on long term incision is most likely restricted to the reaches of the streams below those analysed in this thesis.

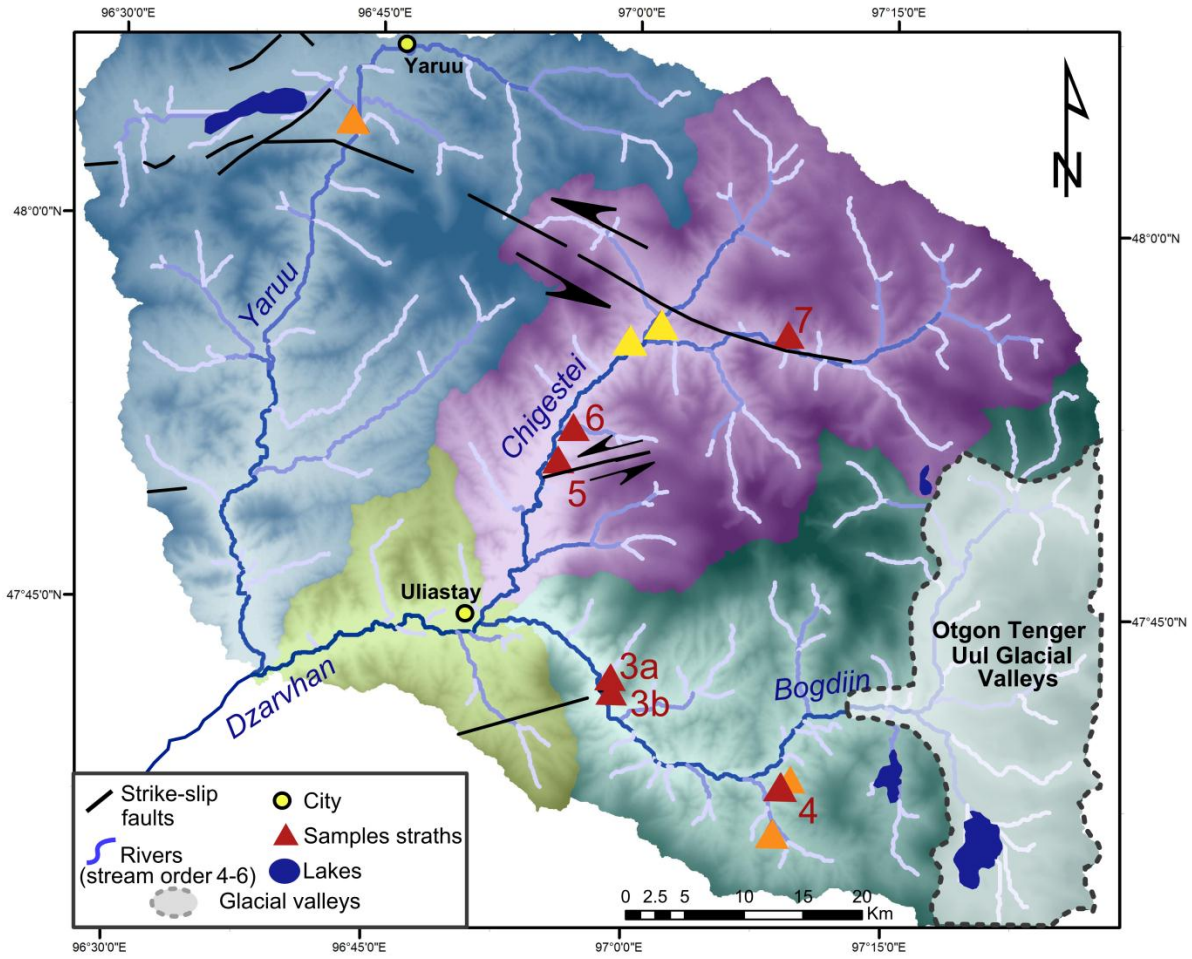

Fig. 2.2. The study area depicted on a 30-m DEM map based on ASTER data. The three streams analyzed are the Yaruu, Chigestei, and Bogdiin which drain into the Dzarvhan river. The drainage areas are differentiated by the different colors of shading of the DEM. Sample locations are shown as red triangles. The Otgon Tenger Uul glaciated valleys are highlighted.

2.2. Strath terraces as tectonic indicators

The utility of terraces in tectonic studies are very useful in deducing history and rates of tectonic deformation of the region. Rivers leave the history of their paleo-longitudinal profiles preserved as strath and fill terraces along the valley walls above the active stream valley (Pazzaglia et al., 1998). River terraces are a geomorphic expression of form and process adjustments in a fluvial system (Figure 2.3). Fill terraces are unconsolidated alluvial sediment with a basal unconformity, typically cut into bedrock, which is the strath (Schumm, 1986; Wegmann and Pazzaglia, 2002). Fill terraces tend to represent responses of the streams to short-term (centuries to tens of millennia) climate change rather than long-term (> 10 ka) tectonic- or base-level induced incision which are recorded by straths. To resolve the question regarding the cause of relief in the Hangay Mountains, bedrock strath terraces along the Chigestei, Bogdiin, and Yaruu streams in western Hangay Mountains have been mapped. Straths along the recorded streams appear to have unpaired terraces indicating lateral erosion as well as continuous vertical incision (Merritts et al., 1994). Lateral erosion is accommodated by pauses in degradation forming strath surfaces, preceded by vertical incision or periods of aggradation. The existence of strath terraces indicates long-term subsidence in Valley of Great Lakes or rock uplift of the Hangay Mountains headwaters.

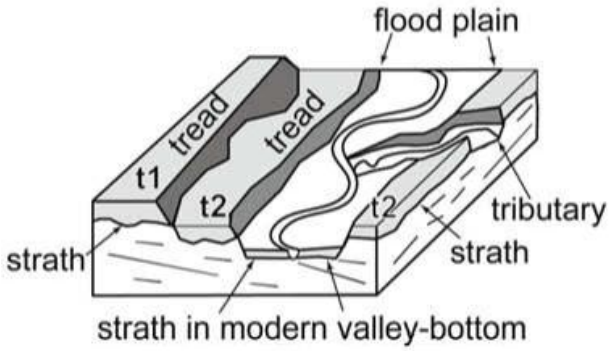

Fig. 2.3. Annotated features of a strath terraces. The strath is cut into bedrock during a period of dynamic equilibrium when the stream is incising horizontally before incising vertically . This creates bench-like geomorphic features. The straths that we sampled had no tread, or sediments from the paleo flood plain. (Wegmann and Pazzaglia, 2009)

2.2.1. Strath Genesis

Timing of strath formation is dependent on climate which can terminate periods of dynamic equilibrium conditions or aid in crossing of thresholds. Dynamic equilibrium can be expressed as a stream attaining a longitudinal profile of minimum gradient after tectonically induced downcutting, therefore allowing the stream to reach a new base level of erosion in a tectonically active reach (Bull, 1990).

$$\frac{stream\ power\ [driving\ factor]}{stream\ resistance\ [resisting\ factor]} = 1.0\ [equilibrium]$$

Aggradation occurs when the resisting power exceeds the driving force, and degradation is when stream power exceeds the resisting factor. Stream power is enhanced by increased tectonic uplift which would increase the slope of the river, which will in turn increase flow

velocity. Incision of the landscape by streams from a rising geological region will induce a fluvial-landscape relief with characteristic V-shaped valley cross-section, or, in the case of extremely rapid incision during which slope erosion was out of equilibrium, a wine glass cross section or significantly convex valley slopes. Rates of tectonically driven incision are dependent on local or regional vertical surface uplift, stream gradient, discharge, availability of sufficiently resistant tools for cutting, and resistance of bedrock. Equilibrium measured by a stream's longitudinal profile ("long profile") is based on a minimum gradient needed to transport the sediment load (Schumm, 1986). Since straths may represent a dynamic equilibrium, we can most likely discover several strath terraces along a valley which preserve the same event of net equilibrium. If we connect strath fragments with similar heights above the channel floor, paleo-long profiles can be created. The stream paleo-long profiles represent the termination of an equilibrium period and the initiation of incision from tectonic processes. We use the modern stream profile as an initial guide to recreate the paleo-long profiles of past channel activity, and decipher a change in incision rate over time (Bull, 1990). However, the correlation of the fragments should be verified with dating or by comparison of clast lithology and soil development on the thin bedload gravels that may survive above the straths.

Stream base-level is defined as the lowest elevation of the stream long profile. The local base-level used in this study is the Valley of Great Lakes, which is an internally drained basin to the west-southwest of the Hangay Mountains. If the Valley of Great Lakes were to subside, then base-level would initiate channel incision creating propagating knick-points upstream. Knick points describe a location along a stream where there is a sharp change in channel slope, such as a waterfall. They result from differential rates of erosion above and below the knick point.

Knick points are created due to the increase in gradient of the stream and subsequently the increase in stream power, although complex responses depend on stream and sediment discharge, rock resistance, and other factors (Schumm, 1993).

Chapter 3: Methodology

3.1. Cosmogenic isotope dating

To determine which processes were responsible for generating relief in the Hangay Mountains, an analysis of three streams in the western Hangay Mountains was undertaken to map paleo-long profiles along the streams and calculate how incision rates varied with time and space. Surface samples of bedrock exposed on strath surfaces were collected for Terrestrial Cosmogenic Nuclide (TCN) isotope dating with ^{10}Be and ^{36}Cl.

3.1.1. Field Sampling

The primary objective is to collect samples from continually exposed surfaces on the straths, ensuring that there is sufficient mass of the mineral of choice (quartz for ^{10}Be, feldspar for ^{36}Cl;Table 3.1). Total masses of purified quartz and feldspar dissolved average 20-25 g, so the sample masses depend on quartz abundance and isotope system used; for ^{10}Be in quartz most samples of granitoids averaged 1.5 kg; for ^{36}Cl in feldspar the samples were half that. When sampling using TCN to date exposure ages of a surface, it is important to consider geometric shielding (if part of the outcrop shields a surface), sample thickness (production rate decreases with depth), evidence of erosion such as gammas (dissolution pits), grain-size relief on the surface, and gurus (weathered-out mineral fragments at the base of an outcrop). At some sites, chemical weathering of the granite created grain-size relief up to 2 cm. Shielding by previous or existing sediment cover, vegetation, and snow must also be avoided or minimized. Uncertainty in these factors will increase the error of the calculated exposure age since corrections will

need to be applied to account for these obstructions to cosmogenic nuclide interaction with the surface. Inheritance of TCN prior to the current exposure history is not likely a significant factor when dating straths because with the possible short episodes of fill cover, the straths are eventually abandoned and continually exposed. Therefore, the chief concern is minimizing the effects of erosion of the bedrock strath. Although fill gravels have probably covered all of the strath surfaces dated, to a cosmic ray, the cobbles and pebbles of the overlying bedload attenuate the cosmic ray flux just as bedrock does., although the variation in erosion rate may be more significant. The thickness of samples collected were ideally within the first 2 cm since this eliminates uncertainty of integrating the cosmic ray flux to greater depths. Many of our samples have a depth between 4 and 7 cm due to the lack of flat surface area needed to collect the required mass.

Table 3.1. Overview of field sample.

Channel	Sample #	Sample Id	Latitude (d.d)	Longitude (d.d	Lithology	Isotope
Bogdiin	**3a**	**MN12-14**	47.69794	96.97589	Granite	^{10}Be
	3b	**MN12-15**	47.69688	96.98092	Granite	^{10}Be
Bogdiin Trib		**MN12-16**	47.60506	97.149	Granodiorite	^{36}Cl
	4	**MN12-17**	47.63228	97.14281	Granite	^{10}Be
		MN12-18	47.63464	97.14483	Granite	^{36}Cl
Chigestei		**MN12-09**	47.93304	97.0202	Granite	^{10}Be
		MN12-11	47.92451	97.00214	Granite	^{10}Be
	5	**MN12-26**	47.84974	96.9294	Granite	^{10}Be
	6	**MN12-27**	47.86578	96.93734	Granite	^{10}Be
Chigestei Trib	**7**	**MN12-28**	47.92894	97.14264	Granite	^{10}Be
Yaruu		**MN12-12**	48.0665	96.72267	Gabbro	^{36}Cl
		MN12-13	48.06677	96.72242	Gabbro	^{36}Cl

Quartz-rich samples were targeted since the production rate of ^{10}Be through spallation and muonic reactions on O and Si is best known on all TCN systems (Balco et al., 2008). Spallation is the nuclear reaction between a highly energetic nucleon with nuclei of exposed atoms, producing numerous particles (muons, nucleons, and larger particles such as nuclides of ^{14}C and ^{10}Be, and other radiation; (Gosse and Phillips, 2001)). During each interaction, the shattering of the target nucleus by the incoming fast cosmic nucleons decreases the average momentum of the primary and secondary (produced in the atmosphere or rock) cosmic ray flux. Immediate disintegration of the target nuclei will occur until the energy of the cosmic ray secondary falls below the binding energy of individual target nucleons. Muogenic production contributes less ^{10}Be than spallation on Earth's surface (muons are charged particles 200X smaller than nucleons so they interact relatively weakly; they account for approximately 2-3% of the total production at the surface, but 50% by a depth of about 4 m in rock because they can penetrate deeper than nucleons). Muogenic interactions that produce TCNs involve the capture of slow negative muons by charged nuclei. Besides having a well characterised production mechanism, quartz is favourable because it is resistant to chemical weathering, is almost ubiquitous, and its stoichiometric formula avoids the complication of additional analyses required of minerals with solid solution compositions, such as feldspar (Gosse and Phillips, 2001).

Unfortunately, many of the straths were not on quartz-rich lithologies. In those instances, cosmogenic ^{36}Cl will be measured in feldspar. While ^{36}Cl dating is not a part of this, it is important to point out the differences in the two systems. The production of ^{10}Be in quartz from spallation and muogenic interactions is better established and because of the longer half-

life (^{10}Be: 1.37 Ma, ^{36}Cl: 0.30 Ma), the ^{10}Be method can date straths as old as 3 Ma without a second isotope, whereas the ^{36}Cl method is limited to about 2 Ma. Besides production by spallation and muonic interactions, ^{35}Cl capture of thermal and epithermal neutrons can produce a significant fraction of ^{36}Cl in minerals, depending on their chlorine concentrations. The latter interactions are reasonably well understood but relative difficult to adjust for geometry effects, moisture content, and periodic snow cover (Gosse and Phillips, 2001).

3.1.2. Strath Geometry

At a large scale, bedrock surfaces on the valley walls that were flat and horizontal over a 100 m^2 and which aligned with other surfaces upstream or downstream on the same valley wall were sought and visited to assess their potential to represent strath terraces. In no valley were straths found laterally continuous over distances of more than a few meters along the valley wall. In fact, all but two straths visited were actually narrow ridges that protruded from the valley wall, with only 10 m wide convex surfaces near the top, before curving down in the upstream or downstream direction. However, the ridges correlated with similar ridge surfaces up and down valley, and some had stream pebbles and cobbles. At the smaller scale, a horizontal surface at least 50 cm from any second face or edge was sought for TCN sampling on each visited strath. Flatness is desired to eliminate unnecessary corrections for self -shielding, and distance from the edge is important to eliminated lost production (Gosse and Phillips, 2001). Bedrock straths can be overlain with sediments from the channel bed, such as gravels. There was no evidence of bedload or fill deposits at our sample sites, although at two locations

rare rounded pebbles were discovered and helped in the interpretation of the surface as a strath terrace. Therefore any unconsolidated gravel that did exist was assumed to have been eroded early after strath abandonment.

3.1.3. ^{10}Be geochemistry

The physical and chemical pre-treatments of the samples was undertaken to separate, concentrate, and purify a sufficient mass of quartz. The samples were washed and/or brushed of undesirable organics, carbonate, and dust. They were then crushed, ground, and sieved into a target size of 150-255 um at the Dalhousie Geochronology Centre (DGC). The sieved fraction was taken through heavy liquids, Frantz magnetic separation, differential leaching in hydrofluoric acid (different dilutions, some in ultrasonic tanks), and air abrasion, until the quartz concentrate had less than 100 ug/mL Al—an indicator of feldspar impurities.

Following quartz purification, the sample was dissolved after adding a known mass of ^{9}Be (typically 10^{19} atoms of ^{9}Be were added), and then taken through the isotope extraction phase of chemistry by G. Yang at DGC (the author viewed and participated in several of the steps). The goal of the isotope extraction phase is to: (1) isolate beryllium isotopes from the quartz and separate them other elements to produce a pure target of BeO for accelerator mass spectrometry (AMS). Important steps are also taken to remove ^{10}B and reduce its contamination because ^{10}B is a significant isobaric interference to ^{10}Be on the AMS (Gosse and Phillips, 2001). While the chemistry normally involves anion and cation chromatography with 2 ml resin volumes, many of the strath samples had high Ca, Na, K, Al, and Ti concentrations, and

consequently large volumes of precipitations. Because of this, extra steps were used to isolate the Be from the other elements (larger resin volumes, and an additional controlled precipitation before the cation chromatography) (Lab notes from G. Yang).

3.1.4. Accelerator Mass Spectrometry (AMS)

AMS is an ultra-sensitive means of counting individual atoms. The AMS achieves this by injecting negative ions of BeO^- into a mass-analysing magnetic field, then dissociating molecular ions and stripping atomic ions of their electrons to create Be^{2+} ions after a first stage of acceleration. Then, following a second stage of acceleration and mass and charge analysis, the AMS detector can identify individual ions (Fifield, 1999). When using AMS, ^{10}Be measurements are almost always normalized to standards of known $^{10}Be/^{9}Be$ ratios (Fifield, 1999; Nishiizumi et al., 2007). The BeO targets prepared for the western Hangay Mountains straths were mixed with ultrapure niobium (which improves the beam current) and packed in stainless steel cathodes, and shipped Lawrence Livermore National Laboratory (LLNL) for analysis of the $^{10}Be/^{9}Be$ (typically samples are at $2x10^{-13}$ and process blanks run at $2x10^{-15}$).

3.1.5. Data reduction

To calculate exposure ages, an online calculator is provided by CRONUS-Earth project funded by the U.S. National Science Foundation (Balco, 2009). The calculator only takes an input of ^{10}Be nuclide concentrations (atoms g^{-1}), rather than the raw ^{10}Be/Be ratio from the AMS. Data reduction is necessary to transform the AMS ratio of ^{10}Be/Be to the ^{10}Be concentration, which is required to calculate the exposure age. To complete this stage, information is needed about the concentration and isotope ratio of the carrier used (275 ug/mL Be, with ^{10}Be/^{9}Be = 1x10^{-18} (extremely low)), the number of ^{9}Be atoms added as carrier, the ratios of ^{10}Be/^{9}Be of the samples and process blanks, and the isotope ratios of the primary standard used in the AMS measurements (Balco et al., 2008; Nishiizumi et al., 2007). The calculator also requires information about the sample location, thickness, shielding, and erosion history to properly adjust the production rate and concentration for the exposure history of the parcel of rock we sampled.

3.1.6. Age interpretation

The cosmogenic exposure ages that are not adjusted for erosion will provide the minimum age of the strath, and therefore an estimate of the time of stream abandonment from the strath. The sampled straths are carved into granite bedrock terraces. At all sampled strath sites there was little or no evidence of overlying gravels. Since the gradient of these channels is low, it can be inferred that an unknown thickness of river gravels was eroded before fully exposing the bedrock strath to cosmogenic nuclides. However, this time of partial shielding of the

bedrock surface by the gravels, (i.e. during which time the bedrock stream bed become abandoned and any bedload has been stripped) is unknown. Therefore the time between stream abandonment and bedrock exposure after the erosion of the river deposits is not accounted for in the exposure ages of the bedrock samples. Considering that no straths visited had an intact bedload cover, it is likely that this duration is small relative to the total exposure time of the strath terraces, particularly the older (higher) straths. Once an exposure age on the bedrock strath is calculated, an addition adjustment must be made for any erosion of the surface since exposure began. Different approaches have been used by others, and the most typical approach is to assume some constant arbitrary erosion rate that was determined independently on similar rocks (Gosse and Phillips, 2001). The approach taken in this thesis is different and takes advantage of the fact that concentrations of radioactive ^{10}Be in very old exposures reach a fixed concentration based on their production (known for the given latitude, longitude, and elevation of the sampled surface), their decay rate (known), and the erosion rate. By assuming that the concentration represents saturation, the concentration defines the long-term erosion rate of that surface.

3.1.7. Uncertainty, precision, confidence

Sources of error are classified as random or systematic. Precision encompasses uncertainties classified as random errors associated with measurement. These include AMS precision, precision of the ICP measurement of the carrier concentration, and precision of the analytical balance (all volumes were transferred gravimetrically). Furthermore, random errors of sample

characteristics include geometry, shielding, thickness, and burial. The strath sample results were not corrected for snow or vegetation cover due to the arid climate, and although it is possible that the paleoclimate was different, we have no information at our sites that indicate snow depth and density, or that there was ever a dense forest cover. For the strath samples, a total analytical precision is calculated from the AMS precision and a 2% precision in all other aspects of the chemistry. . For most samples, the AMS measurement yielded precisions of 2%. The random uncertainty can then be calculated:

$$\sqrt{AMS^2 + chemistry^2} = Random\ Error\ (\%)$$

$$\sqrt{0.02^2 + 0.02^2} = 2.8\ \%$$

The systematic error includes the uncertainty in ^{10}Be half-life, production rate, temporal variation in production rate (cosmic ray flux, geomagnetic paleo-intensity, etc.), and systematic errors associated with ICP and AMS standards (Gosse and Phillips, 2001). To indicate overall accuracy of the age, the random (internal) and systematic (external) errors should be combined in quadrature. However, if only ^{10}Be ages are being used and the systematic errors have not varied significantly, the internal error can be used to characterize the uncertainty of each strath age (and incision rate).

3.2. Paleo-longitudinal profile

Long profiles of the Chigestei, Bogdiin, and Yaruu Gol were created from 30 m resolution ASTER-DEM (Advanced Spaceborne Thermal Emission and Reflection Digital Elevation Model) of Mongolia. The altitude entered in the CRONUS- calculator was measured from the field by GPS (yielding X-Y precision of 10 m on most sites, but Z precision was not sufficient for strath elevations or production rate calibration). Height of the sampled straths above the modern river was measured with hand-held altimeter and verified with laser rangefinder (a precision of 1 m was reproduced between the two methods in the field) to determine TCN production rates and to measure strath heights to compare with heights estimated from remotely sensed data. For correlating the straths from the paleo-long profile, the elevation of the strath terraces, sample sites and modern streams were taken from the ASTER-DEM because less than 10% of the straths were actually visited in the field.

Straths were characterized as 'probable' and 'uncertain' based on the geometry of the terraces. Ideal straths should have horizontal cut-out in the valley face (Merritts et al., 1994) and laterally continuous downstream. As discussed above, most of the straths were not ideal, and therefore it was possible that surfaces identified as straths from the Google Earth or ASTER imagery data were not in fact straths, but were a product of other surface processes (e.g. glaciation, mass wasting, gullying). The straths visited in the field were often preserved on ridges that extended into the valley as preserved features. Similarly, the straths measured on the DEM were all located on ridges. Thus, straths observed on the DEM that were categorised as having probable certainty were larger, flatter, close to similar surfaces with similar elevation upstream or downstream, and not close to evidence of other processes. In all instances,

probable straths were located within 2 km of the modern stream, had a slope less than five degrees, and had a significant width and length (~30 x 30 m^2).

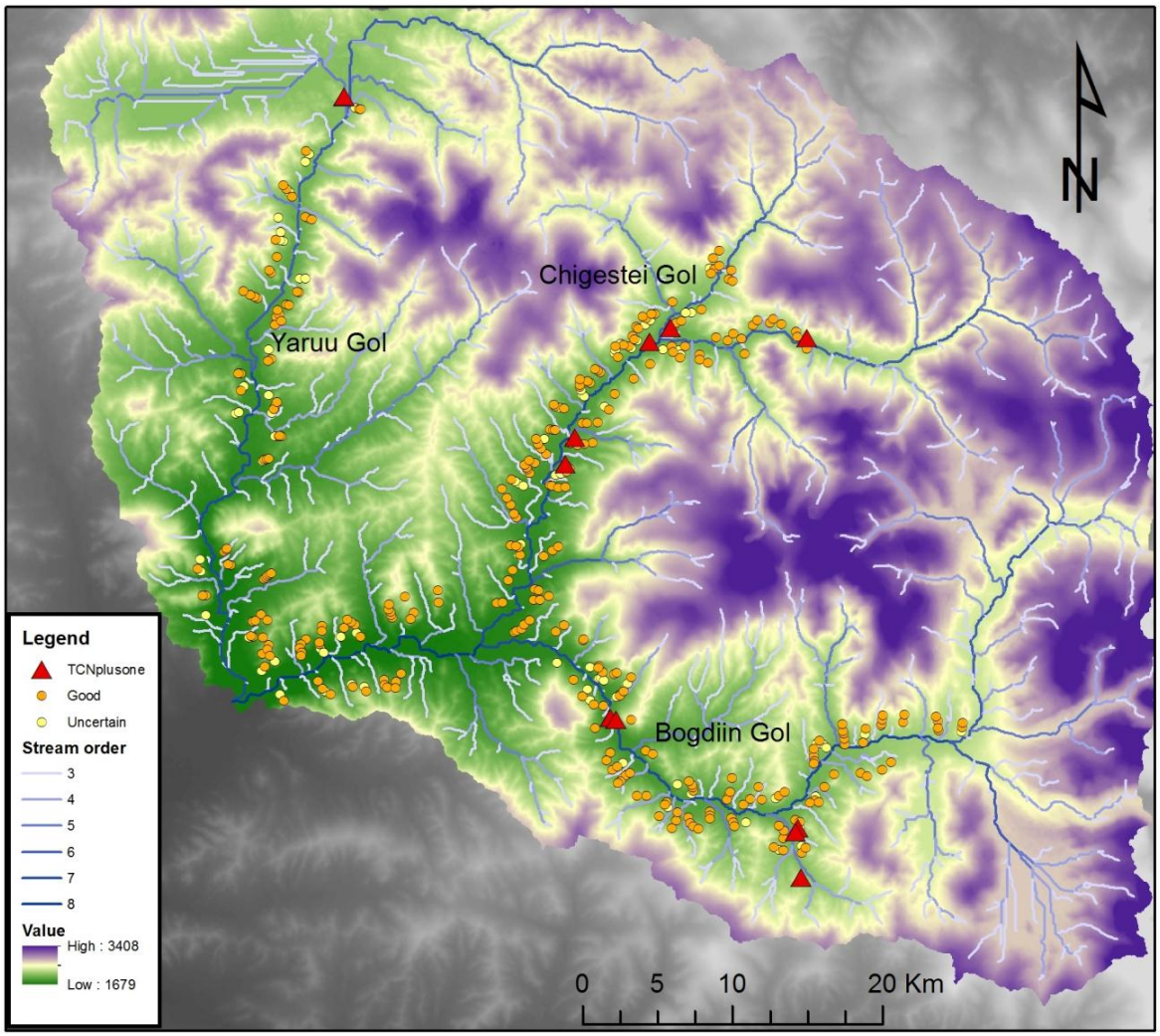

Fig. 3.1. The study area depicted on a 30-m DEM map based on ASTER data. The three streams analyzed are the Yaruu, Chigestei, and Bogdiin Gol. The red triangles are TCN sample sites. The orange circles represent potential strath terraces with a greater degree of confidence (as outlined in Section 3.2), and yellow circles represent potential straths that are less certain due to their steepness, lateral extent, or proximity to areas subject to glacial or hill slope processes.

Straths were characterized as 'probable' and 'uncertain' based on the geometry of the terraces. Ideal straths should have horizontal cut-out in the valley face (Merritts et al., 1994) and laterally continuous downstream. As discussed above, most of the straths were not ideal, and therefore it was possible that surfaces identified as straths from the Google Earth or ASTER imagery data were not in fact straths, but were a product of other surface processes (e.g. glaciation, mass wasting, gullying). The straths visited in the field were often preserved on ridges that extended into the valley as preserved features. Similarly, the straths measured on the DEM were all located on ridges. Thus, straths observed on the DEM that were categorised as having probable certainty were larger, flatter, close to similar surfaces with similar elevation upstream or downstream, and not close to evidence of other processes. In all instances, probable straths were located within 2 km of the modern stream, had a slope less than five degrees, and had a significant width and length (~30 x 30 m^2).

Two methods were used to locate potential strath surfaces along valley walls. Method A used Google Earth 3-dimensional imagery to find surfaces that were strath candidates. Of the straths observed, 62% were characterized as 'probable' straths, and the others were less certain as described above. Method B used the highest resolution of available ASTER-DEM data where straths could be identified based on slope, surface area, and assessment of Google Earth imagery for other criteria as discussed above. With this method, 81% of the straths were 'probable' straths (see Results) and more straths were available for interpreting the paleo-long profiles.

The largest methodological challenge and therefore the thesis method with largest uncertainty was the correlation of strath surfaces. This was because (1) there was insufficient time to verify each strath surface in the field. This would have been important because it would have been possible to date more of the straths; (2) the resolution of the imagery was not sufficient to eliminate some ridges that were incorrectly mapped as straths. Note, the straths visited in the field were often on ridges 3-4 m wide, and 10-12 m long, and thus smaller than the resolution of the DEM data; (3) the number and resolution of exposure ages was insufficient to test the correlations; and (4) the extrapolation of the strath data to interpret paleo-long profiles revealed that multiple interpretations were possible. It is also unfortunate that the straths were not still covered with bedload sediment, which has been used by others (Baker et al., 2009; Wegmann and Pazzaglia, 2002) to help in correlating straths by comparing clast lithology and soil development. Furthermore, it was not possible to quantify the uncertainty in the correlation and interpretation of the long profiles. Thus, while the preferred interpretation is provided, much additional work beyond the scope of this thesis will be necessary to evaluate the methods and confirm the interpretation.

3.2.1. Incision rates

To determine incision rate (*I*) for sites along the river, the method of Lambeck et al. (2004) was employed:

$$\frac{H_S}{T_S} = Incision$$

where H_S is the height (mm of the bedrock strath above the modern channel, and T_S is the age (yr) of the strath preservation in the landscape. Field measurements of *Hs* were made with a combination of laser range finder and hand-held altimetry, and the agreement among them was used to indicate precision, which averaged 1 m. Error in the *Ts* is based on the internal uncertainty of the calculated exposed age according to scaling scheme for spallation by Lal (1991) and Stone (2000). While it is clear that the TCN method cannot resolve years, and the altimeter cannot resolve mm, i.e. the appropriate units of incision should be m/ka based on the methods, the results are presented as mm/yr to be easily compared with the majority of incision rate and erosion data reported in the geological literature.

Chapter 4: Results

4.1. TCN Data

Eight samples were processed for TCN chemistry and AMS analysis. AMS ^{10}Be Standard 07KNSTD was used to normalize the AMS data (see Appendix). Two had high ^{10}B concentrations that significantly interfered with the AMS analysis. The source of the B is believed to be related to construction near the DGC laboratory where the samples were processed, because those two samples were processed at different times than the other samples and there was activity on the 4th floor near where a new wing of the LSC is joining the LSC. Reruns of the two samples were not possible in time for thesis submission. The remaining six targets had high AMS precisions (1-2%). Process blanks had very low measured ratios (2.4 X 10^{-15}). The total blank subtraction was about 3.9 X 10^4 atoms from a range of 4.67 X 10^5 to 1.6 X 10^6 measured boron-corrected atoms of ^{10}Be (see Appendix). The reduced ^{10}Be data in the format for the CRONUS Online Calculator is provided in Table 4.1. The ^{10}Be concentrations range from 8.5 to 32 X 10^5 atoms/g quartz. The shielding factor is ranging from 0.98 to 1 indicating a low shielding effect. The erosion rate was calculated with a no-erosion factor and then calculated for erosion. Erosion of 3.9 mm/ka was used as a basis since the oldest strath reaches saturation at this point, and therefore it was used for all the samples assuming uniform erosion rates on all the strath samples (Table 4.2).

Table 4.1. Reduced ^{10}Be data for age calculation

Erosion Limit	Sample ID	Field ID	Latitude (°)	Longitude (°)	Elevation (m)	Thickness (cm)	Density (g/cm^3)	Shielding factor	Erosion Rate (cm/yr)	Be Conc. (10^5 atom/g)	Be Unc (1) (10^5 atom/g)
NO EROSION	3a	MN12-14	47.69794	96.97589	1904	7	2.6	0.9922	0	32.57	0.77
	3b	MN12-15	47.69688	96.98092	2050	4	2.6	0.9941	0	24.51	0.59
	4	MN12-17	47.63228	97.14281	2046	2	2.6	0.9892	0	10.59	0.28
	5	MN12-26	47.84974	96.9294	2048	2	2.6	1.0000	0	8.561	0.233
	6	MN12-27	47.86578	96.93734	1972	4	2.6	1.0000	0	28.04	0.80
	7	MN12-28	47.92894	97.14264	2153	4	2.6	0.9933	0	21.69	0.71
E = 3.9 mm/ka	3a	MN12-14	47.69794	96.97589	1904	7	2.6	0.9922	0.00039	32.57	0.77
	3b	MN12-15	47.69688	96.98092	2050	4	2.6	0.9941	0.00039	24.51	0.59
	4	MN12-17	47.63228	97.14281	2046	2	2.6	0.9892	0.00039	10.59	0.28
	5	MN12-26	47.84974	96.9294	2048	2	2.6	1.0000	0.00039	8.561	0.233
	6	MN12-27	47.86578	96.93734	1972	4	2.6	1.0000	0.00039	28.04	0.80
	7	MN12-28	47.92894	97.14264	2153	4	2.6	0.9933	0.00039	21.69	0.71

Notes:

Thickness is field measured average thickness of bedrock sample

Density is estimated to be 2.6 g/cm^3; Calculations assumed standard atmospheric model

Be Conc. Is atoms of 10Be per gram of quartz calculated after blank correction

Be Unc is 1-sigma total analytical precision determined by adding AMS and chemistry precisions in quadrature

AMS Standard is 07KNSTD

Table 4.2. Summary of TCN exposure ages

Field ID	Exposure Ages			
	E=0		E=3.9 mm/ka	
	Minimum Age (ka)	Int Unc (ka)	Maximum Age (ka)	Int Unc (ka)
MN12-14	164	4	*Inf*	*Inf*
MN12-15	107	3	179	8
MN12-17	45.1	1.2	53.0	1.7
MN12-26	35.8	1.0	40.6	1.3
MN12-27	129	4	269	22
MN12-28	87.0	2.9	127	7

Notes:

Int Unc is Internal Uncertainty, which includes all analytical precision at 1σ

Inf is infinite age forced by assuming the maximum erosion rate permitted by the measured concentration for sample MN12-15

Ages based on CRONUS-Earth calculator v. 2.1 with constants v. 1.2 and muon v. 1.1

Ages use Lal (1991) and Stone (2000) for scaling of production rates, no geomagnetic field correction

Table 4.3. CRONUS output results

Sample ID	Field ID	Elevation* (m)	^{10}Be† concentration (atoms g^{-1})	1 error‡	Thickness scaling factor§	Shielding factor§	Production rate (atoms/g/yr) spallation	muons	Exposure age# (yr)	Internal uncertainty# (yr)	External uncertainty# (yr)
3a	MN12-14	1880	3.27E+06	76600	0.9452	0.9922	20.33	0.333	164148	4023	15394
3b	MN12-15	2028	2.46E+06	58846	0.9839	0.9941	23.22	0.352	106794	2633	9885
4	MN12-17	1984	1.06E+06	28230	0.976	0.9892	23.39	0.353	45094	1216	4144
5	MN12-26	1957	8.55E+05	23343	0.9839	1	23.78	0.354	35798	985	3288
6	MN12-27	1930	2.81E+06	79991	0.9682	1	22.14	0.343	128761	3794	12159
7	MN12-28	2153	2.17E+07	71097	0.9682	0.9933	25.11	0.363	87009	2915	8256

* Elevation determined in the field with a handheld altimeter, laser and gps

† Be concentrations from

‡ 2% error for AMS and 2% error from chemistry

§ Thickness and geometric shielding factors calculated according to Gosse and Phillips (2001)

Scaling scheme for spallation: Lal (1991)/Stone(2000)

The six samples processed for TCN analysis are summarized in Table 4.4. The distance of each sample from the confluence of the Bogdiin, Chigestei, and Yaruu rivers was calculated from 30 m resolution ASTER-DEM. The modern channel elevation was measured from altimeter and laser in the field. The incision rates were calculated from the elevation above the modern river to the strath and the exposure ages of each sample. The erosion-adjusted rate of 3.9 mm yr^{-1} was used to compare the results of incision rates calculated with no erosion.

Table 4.4. Summary of TCN exposure ages and incision rates

Stream (Sample ID)	TCN Sample ID	Elevation*	Distance from confluence	Modern channel elevation*	Strath height above channel (*d*Z)	Exposure age‡		Incision Rate§			
						*d*T E=0 mm/ka	*d*T E=3.9 mm/ka	*d*T E=0 mm/ka		*d*T E=3.9 mm/ka	
		(m)	(m)	(m)	(m)	(ka)	(ka)	(mm/yr)	(± mm/yr)	(mm/yr)	(± mm/yr)
Bogdiin (3a)	MN12-14	1880	34352	1818	62	164.148	--	0.38	0.01	--	--
Bogdiin (3b)	MN12-15	2028	34708	1818	210	106.794	178.6	1.97	0.06	1.18	0.04
Bogdiin-Trib (4)	MN12-17	1984	51435	1930	54	45.094	53.04	1.20	0.04	1.02	0.04
Chigestei (5)	MN12-26	1957	40025	1815	142	35.798	40.56	3.97	0.12	3.50	0.11
Chigestei (6)	MN12-27	1930	41922	1851	79	128.761	269.3	0.61	0.02	0.29	0.01
Chigestei-Trib (7)	MN12-28	2153	63940	2075	78	87.009	126.5	0.90	0.03	0.62	0.02

Notes

* Strath and channel elevation determined in the field using laser and altimeter

‡ Exposure age calculated from previous table using scaling scheme for spallation: Lal (1991) / Stone (2000)

§ Incision rate calculated from Exposure Age/ Strath Height, so is the average incision rate from strath to present channel elevation

dZ represents the height difference from modern stream to strath (paleo-stream height)

*d*T represents the age of the strath based on its height above the modern stream

4.2. Paleo-longitudinal Profiles

The strath positions were plotted on an elevation vs. stream distance graph (Fig. 4.1. and 4.2.). To extrapolate (correlated) the strath surfaces and define paleo-long profiles, two different approaches were used. In both approaches, the lowest straths (closest to the modern stream) were used to define the lowest paleo-long profile in a given valley. The first approach used Method A of strath identification (with GoogleEarth® imagery). Once the lowest straths were correlated and the first long profile was defined, progressively higher straths were correlated. The correlations were done by eye, with the goal to maximize the number of straths per long profile (and thereby minimize the number of straths used to explain the Method A dataset. During this first attempt, the paleo-long profiles of all three streams were found to converge downstream (Fig. 4.1.).

The second approach was different in two ways. It relied on a greater number of straths (with greater certainty). It also used the modern stream gradient as a guideline for correlating the straths. For the lowest paleo-long profile, the modern long profile was copied and pasted over the straths and tilted slightly to maximize the number of straths that defined the long profile. The next higher strath used that first profile long profile as a guide, but was tilted to maximize the fit. The procedure was repeated until the majority of straths were included on a long profile. The result showed that due to the number of straths, correlation were possible for both convergence and divergence. Bogdiin and Yaruu streams show through the distribution of the straths, a diverging concentration downstream. Alternatively, the Chigestei straths concentration is variable. It appears to be converging downstream, however a large distribution of straths near the confluence lends a diverging trend (Fig. 4.2).

a

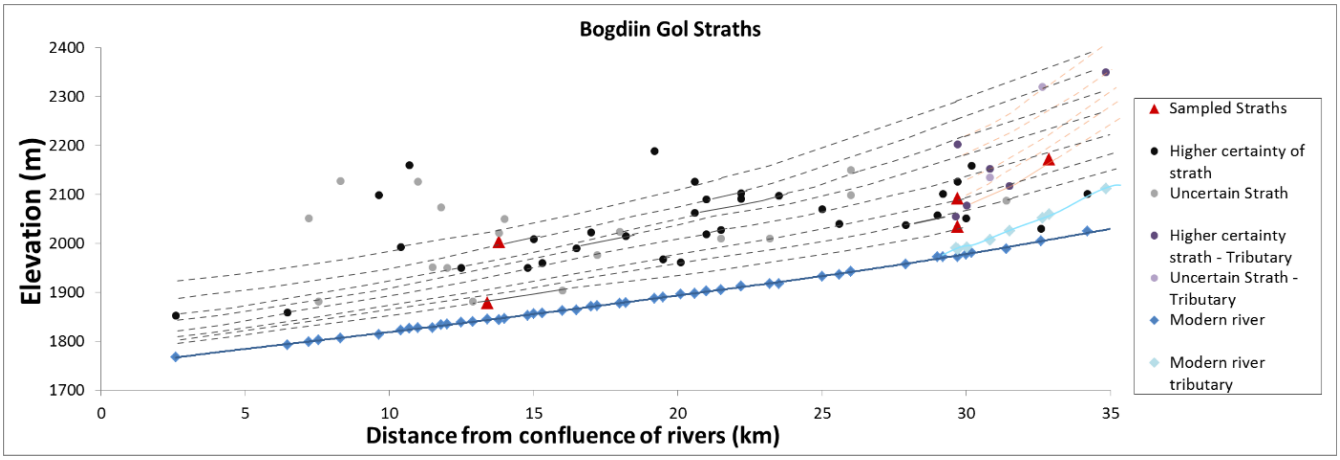

b

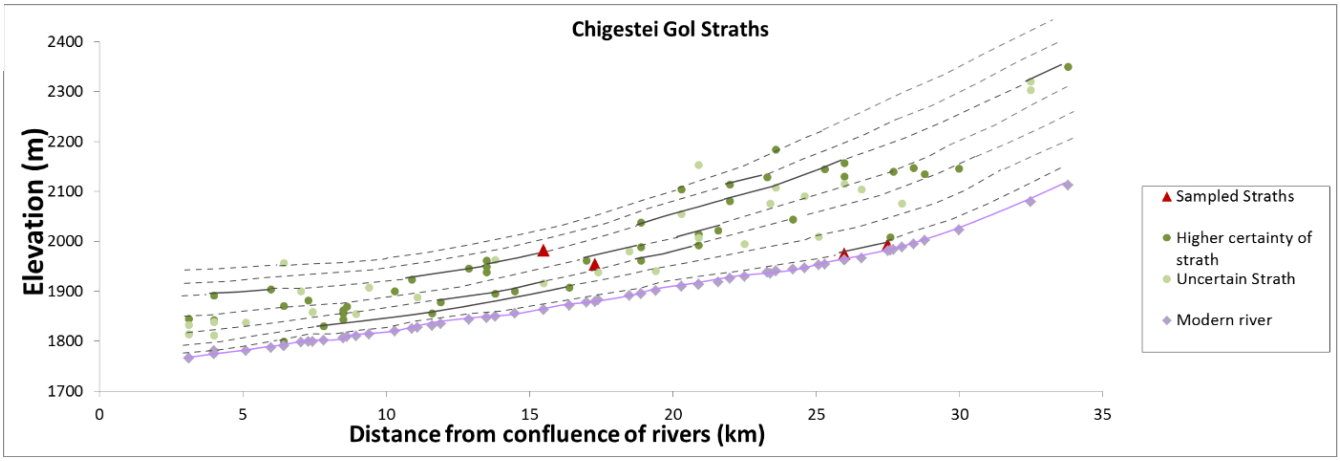

Fig. 4.1. Bogdiin and Chigestei modern and interpreted paleo-long profiles with associated straths based on Approach 1. The profile consists of elevation plotted against the distance upstream from the confluence of the Chigestei and Bogdiin. The strath points were collected with Method A (Google Earth Imagery). The dashed lines represent inferred correlation of the straths, and the solid lines are more certain correlations. Correlation was based on the gradient of the modern river profile at that point form the confluence of the rivers. Correlation showing converging profiles downstream.

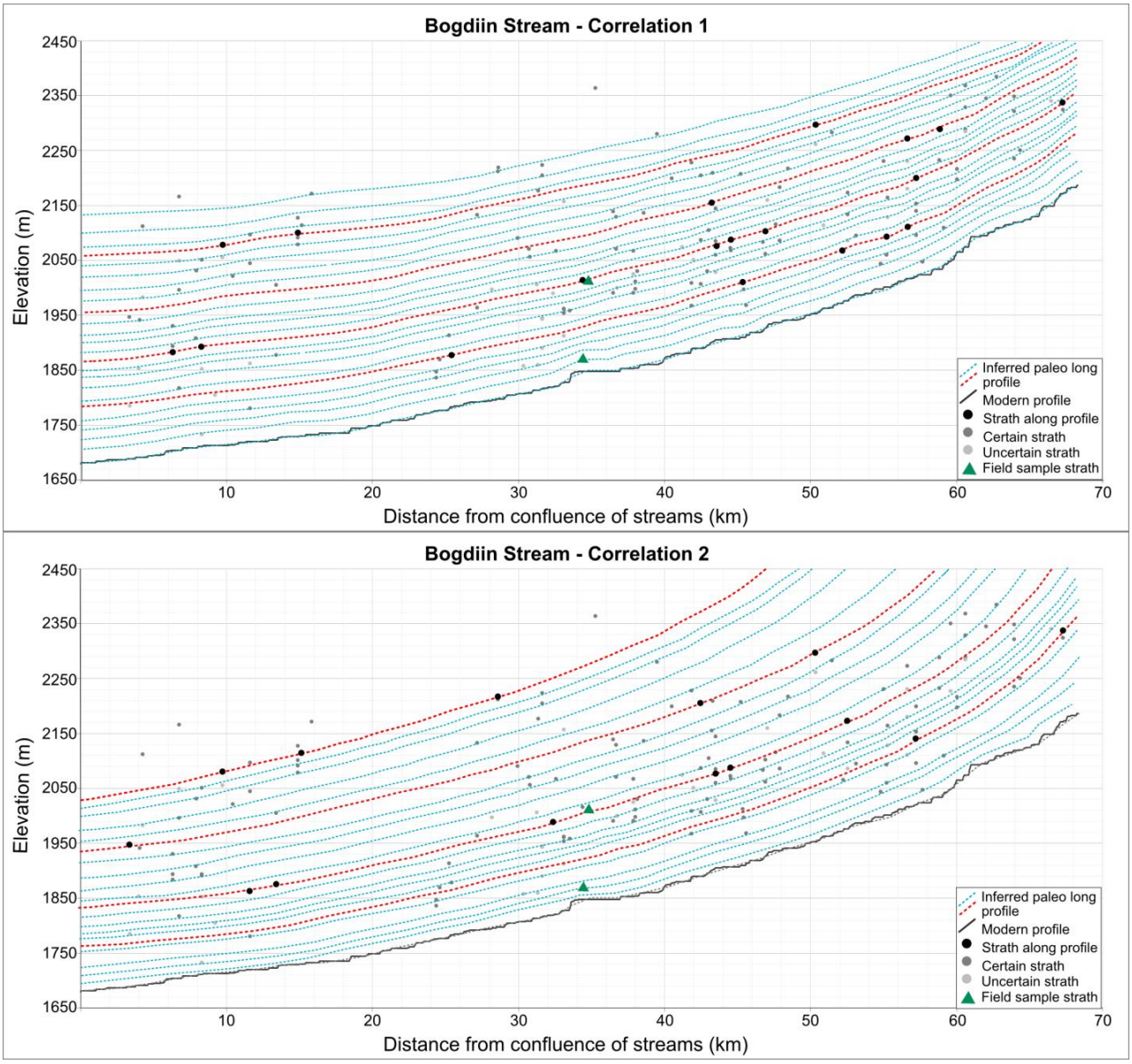

Fig. 4.2. Bogdiin modern and interpreted paleo-long profiles with associated straths based on Approach 2. The profile consists of elevation plotted against the distance upstream from the confluence of the Chigestei, Bogdiin, and Yaruu streams. The strath points were collected with Method B (ASTER-DEM). The dashed lines represent inferred correlation of the straths. The modern profile was used as a basis for correlating the straths. A. (Top graph). Correlation showing an interpretation of diverging downstream profile. B. (Bottom graph) Correlation showing converging profiles. The red dashed lines with black circles highlight the overall trends.

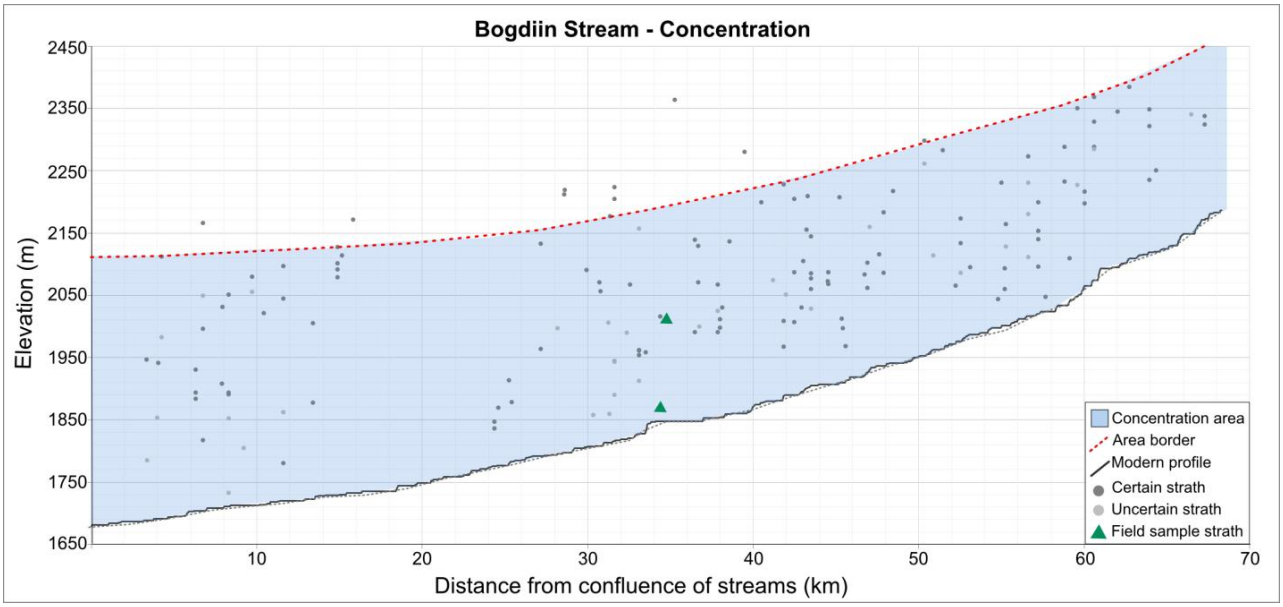

Fig. 4.3. Bogdiin modern profile illustrating concentration of straths downstream. The profile consists of elevation plotted against the distance upstream from the confluence of the Chigestei, Bogdiin, and Yaruu streams. Shaded area contains 95% of the straths points collected by Method B (ASTER-DEM). The shaded area shows the concentration trend of straths is diverging downstream which helps support the inferred paleo-long profiles (Fig. 4.2.). The red dashed line is the boundary of the shaded area, highlighting the overall trend.

Chapter 5: Discussion

5.1. Interpretation of data

The goal of this paper was to determine whether relief was generated by processes of rock uplift or basin subsidence from the analysis of paleo-long profiles along the Bogdiin, Chigestei, and Yaruu headwater tributaries of the Dzarvhan River. Attempts of correlation of the straths in each valley reveal that the correlations are very interpretive, and no unique solution was determined for either of the three valleys. Without soil information, gravel provenance, or more age control to assist in correlation, it was impossible to distinguish net convergence or divergence (uplift or subsidence respectively) of paleo-long the paleo-long profiles (Fig. 4.2). Most strath data points were never confirmed in the field as a result of limited field work in the region, therefore the level of uncertainty related to the ASTER-DEM and Google Earth methods is high. The locations of the sampled straths were often on narrow (3-4 m wide by 10-12 m long) ridges, suggesting the straths have experienced significant erosion if they were originally laterally extensive for more than a few meters. Additionally, the lack of bedrock surfaces on the straths with fluvial polish or potholes, and the lack of bedload overlying the visited straths, supports the notion that the straths have been eroded.

However, despite these challenges, this section will show that (i) paleo-long slight divergent-downstream interpretation of the paleo-long profiles is apparent; (ii) the incision in the region is slow; (iii) the Bogdiin and Chigestei show similar patterns of incision rate; and (iv) the influence of strike-slip extensional step-overs on the streams that is observed in the modern long profiles is not observed in the strath data.

5.1.1 Paleo-longitudinal Profiles

The method of identifying strath surfaces from remotely sensed data for the Chigestei, Bogdiin, and Yaruu valleys has identified 365 surfaces that were interpreted to be straths. Unfortunately, only 12 (3%) of the straths were visited. Without field confirmation, it is difficult to evaluate the robustness of the dataset. Since many of the sampled straths and satellite imagery picks were on narrow ridges as opposed to broad 3D planar surfaces (Baker et al., 2009; Vassallo et al., 2007b; Wegmann and Pazzaglia, 2002), it is not possible to preclude that some of the ridges were formed from processes other than lateral planation, such as hill slope processes, glaciation, or gullying. Only 2 of the 12 straths visited had rounded pebbles interpreted to be stream gravels. Those gravels were isolated patches of sands and granules with rare pebbles (1 or 2 pebbles per strath), presumably erosional lag from bedload that once covered the strath surface. Without documented evidence such as bedded stream gravels or fluvial polishing of the bedrock surface, it is not possible to confidently link the identified surfaces to lateral planation by streams. Therefore, additional field mapping will be required to assess the validity of the identification of the surfaces as straths, and furthermore the validity of the interpretation of the paleo-long profiles and their relationship to regional incision or rock uplift.

The preferred method of correlating the straths of the Chigestei, Bogdiin, and Yaruu was Method B (ASTER DEM) because it provided more straths that were more widely distributed along the entire lengths of the three valleys. Correlating the straths using the modern profile of the streams to guide the lower long profiles seem to provide the most reproducible pattern.

Although the Bogdiin, and Chigestei had numerous straths along each valley to correlate, the exposure ages were not helpful since there were too few ages and they were not distributed along the valley. The ^{10}Be exposure ages were compared with the paleo-long profile interpretations but did not significantly aid in testing the validity of the long profiles because of the paucity of ages and their uncertainty as discussed above. The Bogdiin and Chigestei had 108 and 97 straths respectively, and the Yaruu stream had 49. This discontinuity in distribution is most likely due to the differing lengths of the streams. The Yaruu is the shortest stream at 54.1 km, and the Bogdiin and Chiestei are 68.3 km and 72.7 km respectively.

The similarity in modern profiles of the Bogdiin and Chigestei stream could be attributed to their once shared drainage of the Otgon Tenger Uul mountain, which was glaciated in the last glaciations. Presently, only a tributary of the Chigestei stream drains a lake blocked by a lateral moraine (Fig. 2.2). The Yaruu's modern profile is significantly steeper than the Bogdiin and Chigestei (Fig. 5.1). The Yaruu stream runs north-south and crosses several possible left-lateral strike slip faults (Walker et al., 2008).

Of the different approaches attempted to correlate strath elevations, only the first—which was based on strath identification method A—suggested that the paleo-long profile gradients diverged downstream. The pattern of paleo-long profiles using the second approach, involving the ASTER data and using the gradient of the modern profile to guide correlation, indicates ubiquitous downstream divergence in all streams (Fig. 4.4). Not only does it appear that the stream long profile gradients get steeper over time, but all three streams show the same pattern. The interpretations from Method A and B differ for several reasons: (i) Method A has

fewer strath picks and the ratio of 'probable' to 'uncertain' straths was low; (ii) the resolution of the Google Earth imagery is variable from block to block making it difficult to locate straths in zones of low resolution.

Furthermore, the downstream divergence interpretation using Method B (ASTER-DEM) is preferred based on (i) the greater number of straths connected in the diverging correlation compared to the converging correlation (Fig. 4.1a vs. Fig. 4.2); (ii) the distribution of straths along the Bogdiin and Yaruu appears to widen downstream (Fig. 5.1 and 5.3); and (iii) Bogdiin, Chigestei, and Yaruu share a uniform pattern of correlations based on the two previous points.

Assuming that the downstream divergence of paleo-long profiles model is correct, this indicates that basin subsidence, not headwater rock uplift, is mostly responsible for the incision and relief generation of the Hangay Mountains. It may be possible to establish a timing of the tectonic activity affected the stream profiles once a better chronology is developed (see future work).

Other relationships between tectonics and stream profiles can be inferred. The flat profile in the headwaters of the Yaruu stream is inferred to be the result of the pull-apart basin about 10-12 km wide from a step-over strike slip fault (Fig. 2.2). At other locations, there are tentative strike-slip faults crossing the Yaruu and the Chigestei respectively (Walker et al., 2008) which forms small extensional basins, widening the valley floodplain in both cases (Figs. 5.1; 5.2; 5.3). The Chigestei stream gradient is not highly affected by the small extension which widens the floodplain from 0.5-1.6 km. However, the Yaruu stream flows almost directly north to south, and crosses many possible strike-slip faults described by Walker et al. (2008) which appears to

affect the modern long profile (Fig. 5.3). It is difficult to determine the initial timing of these faults from the paleo-long profiles due to the lack of constraining straths in these locations.

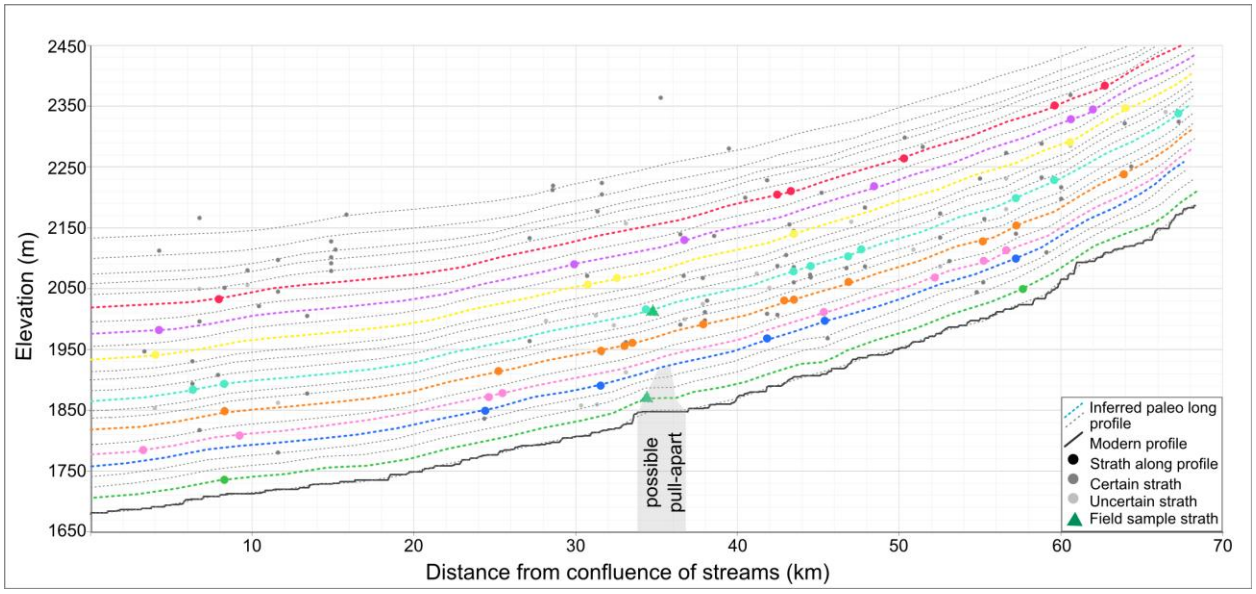

Figure 5.1. Bogdiin modern and interpreted paleo-long profiles with associated straths based on Method B (ASTER-DEM). The colored paleo-long profiles shown in this diagram are the best fit interpretation which contain 6-8 straths along each line. The grey shaded area is an inferred pull apart basin based on possible strike slip step over extension from imagery (Walker et al., 2008) the shaded area continues into the paleo-long profiles indicating the evolution of the strike-slip. The product of the step-over would be a larger valley and a flat gradient.

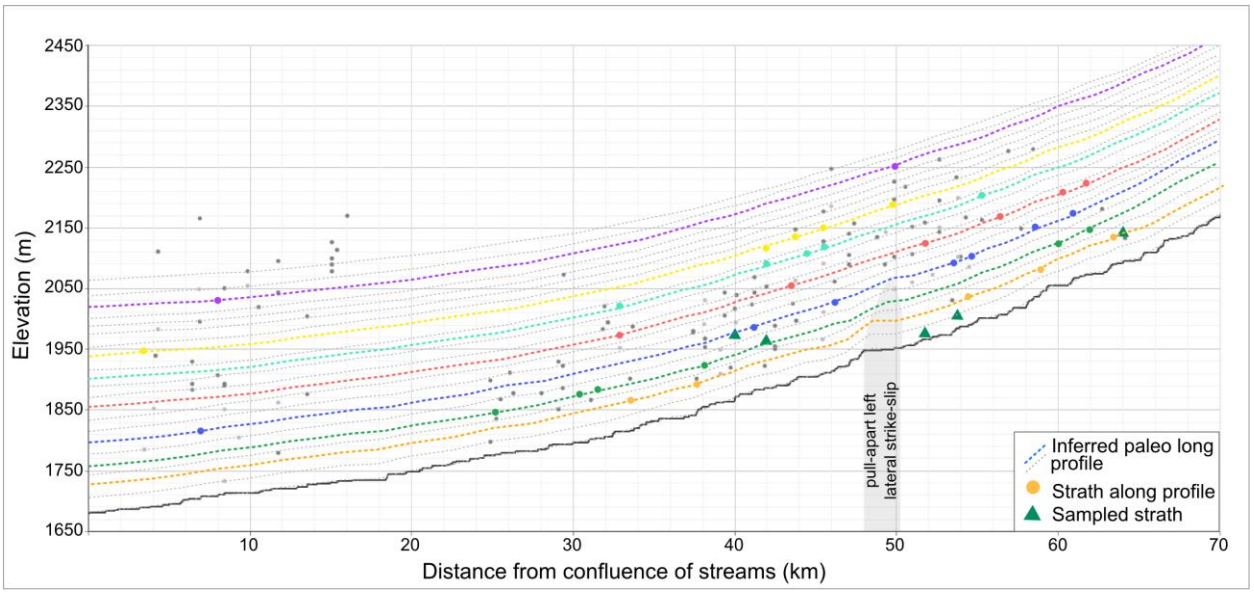

Figure 5.2. Chigestei modern and interpreted paleo-long profiles with associated straths based on Method B (ASTER-DEM). The colored paleo-long profiles shown in this diagram are the best fit interpretation which contain 6-8 straths along each line. The grey shaded area is an inferred pull apart basin based on possible strike slip step over extension from imagery (Walker et al., 2008).

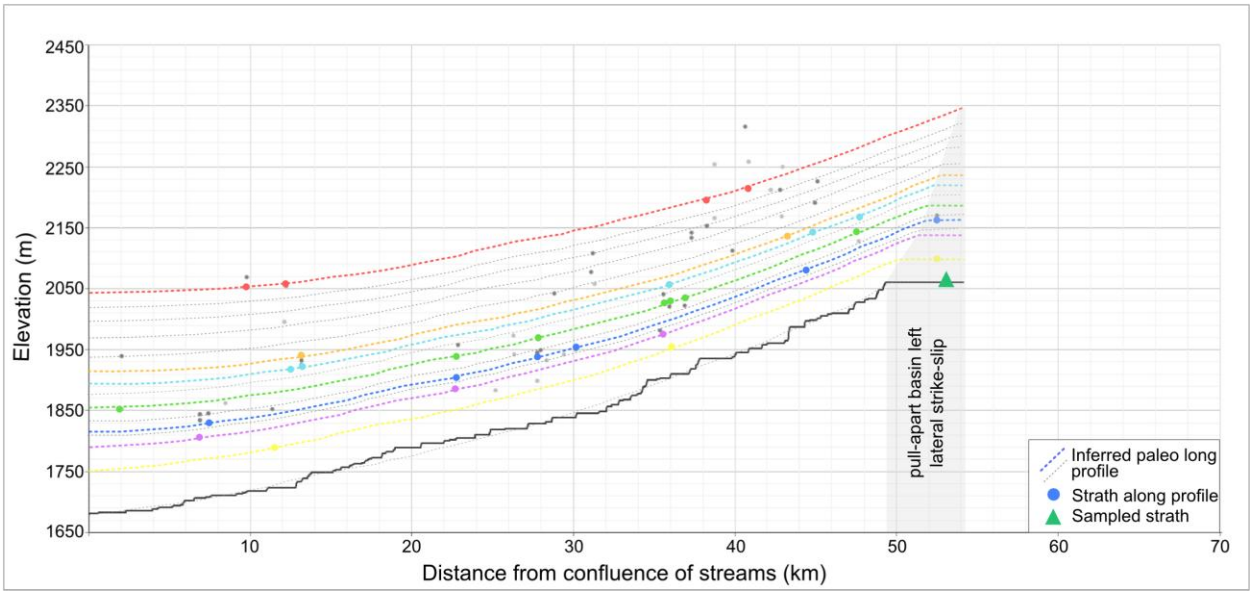

Figure 5.3. Yaruu modern and interpreted paleo-long profiles with associated straths based on Method B (ASTER-DEM). The colored paleo-long profiles shown in this diagram are the best fit interpretation which contain 6-8 straths along each line. The grey shaded area is an inferred pull apart basin based on possible strike slip step over extension from imagery. The pull-apart basin near the headwaters of the Yaruu is 10-12km wide, with active ongoing slip, with a total displacement ~12 km(Walker et al., 2008).

5.1.2 Exposure ages of field samples

The ^{10}Be exposure dates provide a means to estimate the exposure duration of each strath. However, as was discussed in the methodology and results chapters, it was not possible to constrain the erosion rate for each surface during exposure. The ages based on zero erosion rate are minima, and therefore offer minimum limiting age-constraints for the straths.

To adjust for erosion, the unique constant erosion rate required to achieve secular equilibrium concentration for the sample with highest concentration was determined to be 3.9 mm/yr. Modelling for erosion accounts for overlying terrace bedload gravels that have most likely eroded away since stream abandonment of the strath. The erosion-adjusted ages provide an older age of the samples. The erosion rate was determined as the highest possible before sample 3a appears oversaturated (displays an age of infinity). Exposure ages adjusted for this erosion rate provides a closer estimate of the exposure duration for each dated strath, but it is uncertain if the erosion rate is the same on each surface, if the erosion rate was constant over time, and what role bedload cover had on erosion history or shielding. While the number and position of the samples are insufficient to provide a stratigraphic test on the quality of the strath chronology, in two instances straths at higher elevations above the modern stream yielded significantly lower ages (sample 3a and 3b for the Bogdiin river, and sample 5 on the Chigestei river). While the ages may reflect different incision rates for different parts of the stream, it is also possible that the younger age of each pair is more affected by erosion than estimated. Thus, while the ages that are not adjusted for surface erosion are by definition

precise minimum ages, the uncertainty in each incision rate based on the erosion-adjusted age is difficult to evaluate.

Strath exposure ages should increase with height above the channels. Along the Bogdiin, sample 3a and 3b are located along the same ridge, and sample 4 is 9.8 km upstream. Sample 3a has a no-erosion age of 164±4 ka (erosion-adjusted age is infinity) and 62 m above the stream. Alternatively, sample 3b is along the same ridge at 210 m above the stream with a no-erosion exposure age of 107±3 ka (erosion-adjusted age is 179±8 ka). Along the Chigestei, sample 6 and 7 have an exposure age of 129±4 ka and 87±2.9 ka and lie at 79 and 78 m above the modern stream. Alternatively, sample 5 has an age of 35.8±1 ka at 142 m above the modern stream, which seems highly unlikely, as it would invalidate the other two samples along this valley.

The invalidity of sample 3b and 5 is based on several factors. Firstly, the location of the collected samples (smaller straths), secondly, exposure ages are easily younger since erosional processes could strip the originally surface, and lastly, the LGM moraine (Lehmkuhl et al., 2004) which lies 1.8 km upstream the Bogdiin from the last measured strath is only 10-15m above the modern stream. Therefore, for the remainder of the discussion, sample 3b and 5 will not be considered in evaluation of the data, and the erosion-adjusted age will be used for the remainder of this discussion.

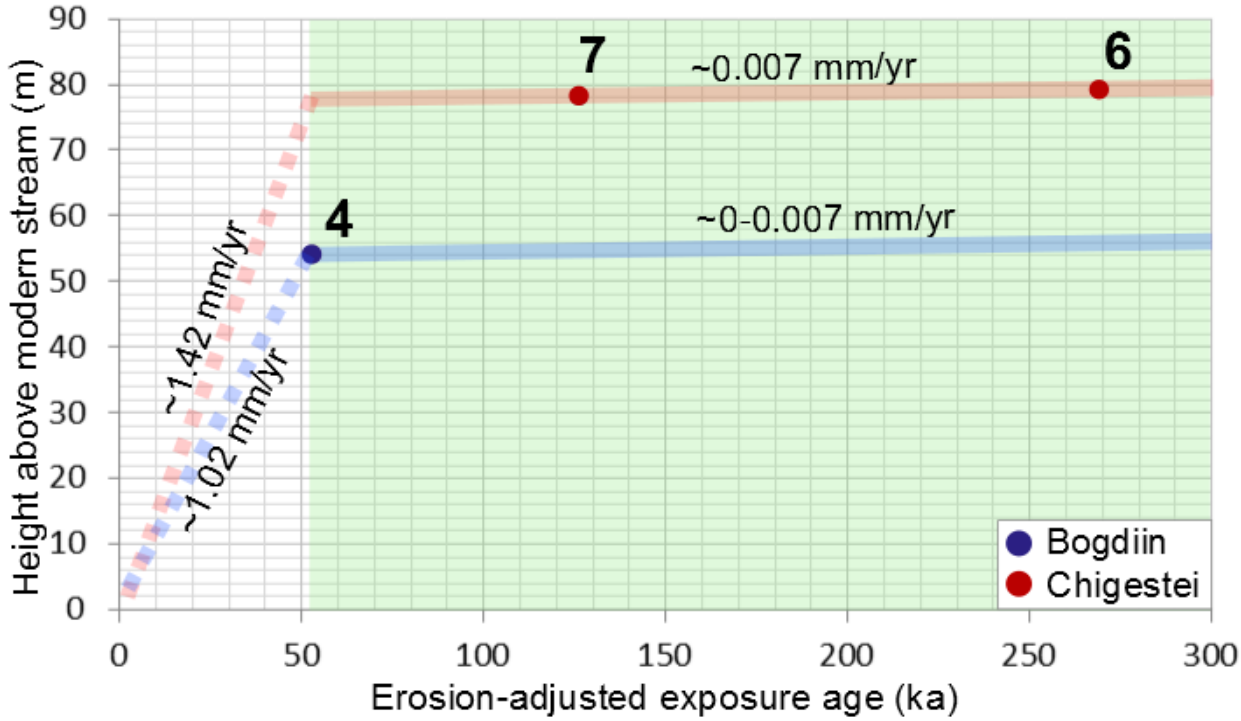

Fig. 5.4. The incision rate results (Fig. 5.4) and the position of suggest that incision rate was low. This indicates that the Bogdiin stream was ~25 m lower than Chigestei stream. This could be a product of drainage area, sediment influx, and the power of the streams. Between the abandonment of the strath at site 3 and present, Chigestei had to incise a greater height than Bogdiin.

The ^{10}Be exposure ages of samples were used to calculate the incision rate from sampled strath surfaces to modern stream level. The incision rate was first calculated from modern stream level to each sampled strath (Table 4.3). This method yields several incision rates that are very high relative to rivers in similar tectonic settings, and a wide range of incision rates (0.29±0.01 mm yr^{-1} to 3.5±0.11 mm yr^{-1}). For instance, when compared to the Rio Diamante in the Argentine flank of the Southern Central Andes with an incision rate of 0.1 to 5 mm yr^{-1} (Baker et al., 2009), the Hangay Mountains incision rates based on ages that were not corrected

for erosion seem excessively fast. Furthermore, the range in rates suggests that the incision rates should not be calculated for every strath to modern stream, but rather that it is necessary to explore the possibilities of changes in incision rate over time, i.e. over the time periods represented between straths.

The erosion-adjusted ages provide a more realistic estimate of incision rate (Fig. 5.4), although the uncertainty in the magnitude and variability of erosion rate is unknown. The uncertainty in the thickness and persistence of any bedload above the sampled straths contributes significantly to this error. The high incision rate of the original calculated incisions rates (Table 4.3) is unlikely, considering that this region has coarse igneous bedrock, and currently a relatively low annual precipitation (209 mm/yr) that is mostly evenly distributed throughout the year. In contrast, incision rates up to 1.2 mm/yr are common in tectonically active regions such as the Olympic Peninsula in western Washington State with much higher annual rainfall (>1500 mm/yr) to support a temperate rainforest, double the relief of Hangay Mountains, and less resistant rocks (Eocene greywacke) (Wegmann and Pazzaglia, 2002). Alternatively, the sampled straths were plotted height above stream compared to exposure-adjusted ages (Baker et al., 2009; Leland et al., 1998)(Fig. 5.4). The incision was then calculated between straths of a given river. The Chigestei incision rate between samples 6 and 7 is 0.007 mm yr^{-1}. Sample 4 is not displayed because the adjustment for erosion causes saturation of ^{10}Be, and thus the age is indistinguishable from infinity. If the incision rate is calculated for the Bogdiin stream, using the erosion-adjusted exposure age (infinity), the incision rate between 3a and 4 would be ~0 mm yr^{-1}. These rates represent a maximum incision rate, since the erosion-adjusted ages are minimum exposure ages for the surface. Therefore, incision rates before

53.0±1.7 ka (sample 4), are between ~0 - 0.007 mm yr^{-1} which is comparable to the incision rate from Eocene to Miocene of the Sierra Nevada during uplift (0.007 mm yr^{-1}) (Wakabayashi and Sawyer, 2001), and the Yellow River channel profile and basin-wide average erosion rate of 0.007 mm yr^{-1} as a result of a combination of base-level fall and differential uplift in the headwaters (Harkins et al., 2007).

Since the constant incision does not extrapolate to the present modern day level on two of the studied rivers (Fig 5.4), it appears that the rate of incision has changed over time. The first period (shaded green) represents an average incision rate spanning ~250 ka to infinite. This would be followed by a faster incision rate of 1.42 – 1.02 mm yr^{-1} over the last ~50 ka. There are two explanations of this change. The first could be that there has been a significant tectonic process of uplift or subsidence since 50 ka changing the controls of the river. Alternatively, the 50 kyr span is only capturing the incision rate component of a long-term cyclic incision history. For example, the increased incision could be due to the impact of glaciations, or a period of faster drop in base level during the past 50 ka relative to the preceding 3 Ma. In the latter explanation, the overall average of the incision rate can be constant over long time periods, but appears to be high closer to present day since we are capturing a portion of a long-term cycle, which in the greater scheme is not significant (Baker et al., 2009; Pazzaglia et al., 1998; Wegmann and Pazzaglia, 2002). Since the slopes of incision rates of the Chigestei and Bogdiin streams are similar (Fig 5.4), the incision history may be similar for both channels.

5.1.3 Initiation of relief generating incision

Since the incision rates on the Bogdiin and Chigestei are comparable, it is reasonable to extrapolate the initiation of incision based on the height of known samples and their erosion-adjusted ages, and the height of the tallest straths identified in Method 2 (ASTER-DEM). The projected ages can be calculated using the erosion-adjusted incision rates and the average height of the tallest strath (~400 m). Therefore, the erosion-adjusted projected minimum ages of these straths with the maximum incision rate of ~0 - 0.007 mm yr^{-1} is minimum ~57 Ma.

5.2. History of the generation of relief of the western Hangay Mountains

Based on these interpretations and assuming Yaruu also displays similar incision rates, the process governing the relief generation appears to be large scale (perhaps the entire plateau) as opposed to local individual-driven controls on each river. Assuming the average incision rate has been roughly constant from the period of incision (~0-0.007 mm yr^{-1}), it would have taken a period of 30 million years to incise from our highest sampled strath (210 m at sample site 3b) to the modern stream level. Therefore, the paleo-long profiles and incision rate argue that the western Hangay relief is generated from a gradual drop in base-level at a very slow rate.

5.2.1 Model of Incision for the western Hangay Mountains

A conceptual model of the incision history of the Hangay Mountains is proposed based on the strath and geochronology data provided, but also considering other data available at the time of writing this thesis. In this model, generation of high elevation and relatively high relief are considered to have resulted from two separate processes. The high elevation in the region of the Hangay Mountains is considered, firstly, as a product of a surface uplift event due to mantle delamination supported by (i) tomographic data (Barruol et al., 2008; Kulakov, 2008; Yarmolyuk et al., 2013) and (ii) basalt geochemistry surrounding the Hangay and Mongolia (Barry et al., 2003; Kovalenko, 2010); and secondly, as a result of the resistance of the granite of the Khangay batholith within the Hangay Mountains (Benedict, 1993). It appears that the Hangay Mountains achieved much of their rock uplift much before the last few million years, perhaps when the Mongolian Plateau was derived, based on the slow erosion rates measured (correction for erosion would make the ^{10}Be ages older and therefore the rates even slower). The generation of relief is considered to have been slow. Although no significant headwater rock uplift or base-level fall is evident from the strath record, relief generation from base-level fall (based on weak evidence of downstream divergence) is interpreted to have resulted from a combination of Baikal Lake rifting, and the formation of compressional and successor basins forming in the Valley of Great Lakes (Cunningham, 2005; Sladen and Traynor, 2000).

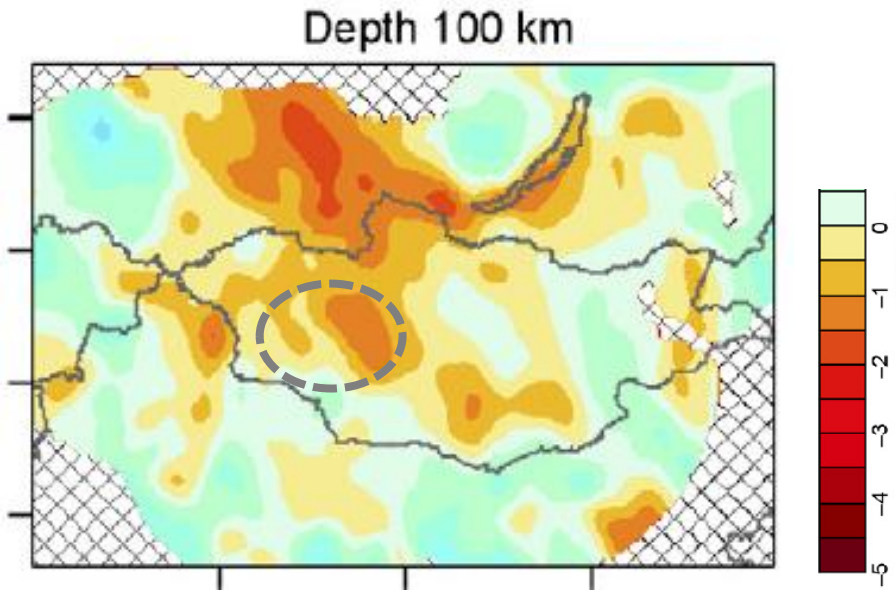

Fig. 5.5. Velocity anomalies obtained by ITS inversion of real data from southern Siberia and Mongolia. Circle contours Hangay Mountains. The scale on the right is velocity anomaly (%)(Kulakov, 2008).

Mantle tomography (Fig. 5.5) suggests lithosphere thickness is thinner from Siberian Craton to the Valley of Great Lakes and Altai Mountains in southern Mongolia (Barruol et al., 2008; Mordvinova et al., 2007). A popular model proposes an intracontinental hot spot as the cause of uplift of the Hangay Mountains (Kovalenko, 2010; Yarmolyuk et al., 1995). However, the model of deep rooted mantle plume lacks significant evidence to support the volcanics and the uplift in the Hangay, based on (1) diffuse nature of the volcanism, (2) ages are not progressive throughout the Cenozoic, (3) the volcanism is not continuous and small in volume, (4) mantle xenoliths do not exceed 1100C (Ionov et al, 1998), (5) the lack of geophysical evidence of a deep plume, (6) absence of high heat flow, (7) and no flood basalt province (Barry et al., 2003).

5.2.2 Interpretation

Several interpretations have been made to explain the high elevation and landscape of the Hangay Mountains (Barry et al., 2003; Cunningham, 2001; Walker et al., 2008). In this section, a speculative interpretation has been made to propose the forces that contributed to the elevation of the mountains and regionally uplifted area, as well as to propose a the cause of base-level fall (Fig. 5.5).

a) In the Late Permian – Middle Triassic, the Mongol-Okhotsk subduction under Mongolia emplaced calc-alkaline granitoids of the Khangay batholith. The Hangay Mountains lithology is mostly the Khangay granodiorites (Donskaya et al., 2013).

b) The Khentey batholith, located to the east of the Hangay Mountains, is a calc-alkaline granitoid similar to the Khangay batholith emplaced in the Middle Triassic – Middle Jurassic as the Amurian superterrane docked with Mongolia. The Khentey batholith is the dominant lithology of the Hentiyn Mountain range in northern Mongolia (Donskaya et al., 2013).

c) The Jurassic is characterized by a significant decrease in magmatic activity in Siberia associated with late stage subduction (Transbaikalia, Russia). The Mongol-Okhotsk Orogony was formed from the collision of Mongolian terrane and Armurian superterrane (Donskaya et al., 2013).

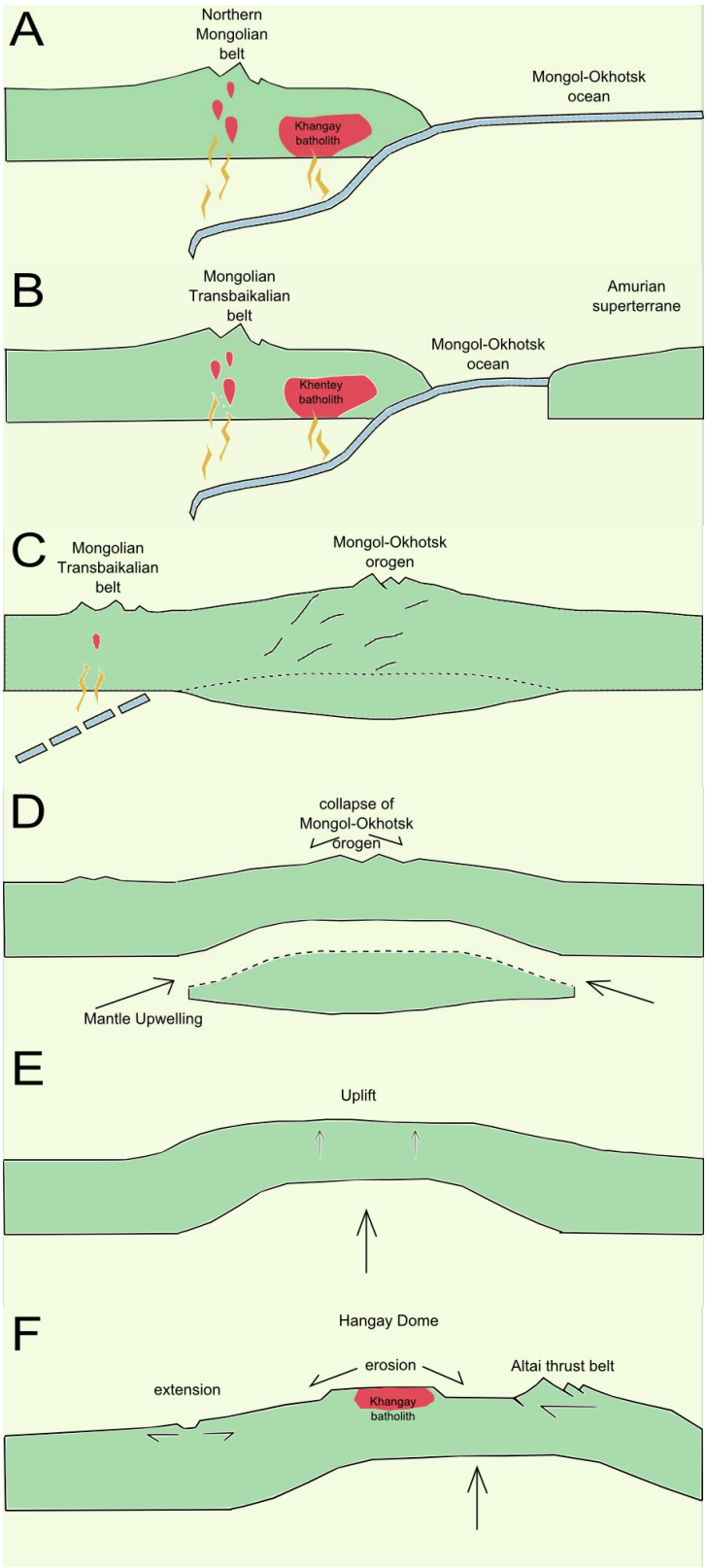

Fig. 5.6. Cartoon illustrating the origin of the high elevation and the subsequent incision of the Hangay Mountains from basins forming in the Valley of Great Lakes. See text for details.

d) During the Cretaceous, the Transbaikalia and Mongol-Okhotsk orogens collapsed from erosional processes (Avouac and Burov, 1996) exhuming the Khangay batholiths closer to surface. This period is also characteristic of Cenozoic volcanism. Basalts are located in several areas surrounding the Hangay Mountains, and geochemical data indicate the lithosphere has not yet been thinned (Barry et al., 2003; Kovalenko, 2010). Magmatism through central Mongolia has taken place for the last 150 Ma, however the largest periods of outburst were in the Early Cretaceous and the Miocene (Yarmolyuk et al., 1995) although the Hangay Mountains did not experience Cenozoic volcanism. The geochemistry of the basalts gave controversial results, indicating the source is normally associated with contamination of the aesthenosphere by a deep mantle plume, or by delamination of the continental mantle lithosphere (Barry et al., 2003; Kovalenko, 2010). Since the mantle plume model lacks support, Barry et al. (2003) suggests lithospheric weakening or delamination coupled with replacement by aesthenospheric melts. Therefore, the Late Cretaceous could be associated with the onset of mantle delamination, and lithospheric weakening from the anomaly created from the collision of the Armurian superterrane docking into Mongolia.

e) From the period of Late Cretaceous to Miocene, Mongolia's sublithosphere is delaminated, and aesthenospheric melts upwell under Mongolia causing uplift of a large region. Geochemical analysis of the Hangay basalt composition indicates the parental magma could be from shallow asthenosphere with lithosphere or crustal contamination. Mongolian lavas were generated from small amounts of partial melting, and it is thought that melting

most likely occurred close to the base of the lithosphere, or was even sublithospheric (Barry et al., 2003). Therefore, by the time the second stage of volcanism occurred in the Miocene, the lithospheric situation under Mongolia had changed since the geochemical analysis of the Cretaceous and Miocene basalts indicate two opposing sources.

In support of large regional scale uplift, many of the peaks in the field within the Hangay Mountains are flat topped, often with the presence of felsenmer surfaces. The Gobi-Altai range started to grow ~5±3 Ma as a response to far-field India-Eurasian, many of the peaks are flat summit plateaus. The plateaus are the oldest known tectonically uplifted surfaces on Earth, which was determined through apatite fission track dating of the Gobi-Altai summits. The preservation of these summits is attributed to the dry climate (Jolivet et al., 2007). In the Gobi-Altai range, the mountains are subsequently uplifted from brittle deformation at a steady rate to preserve the plateau summits (Vassallo et al., 2007a).

At this point, the Hangay is a relatively low relief high elevation plateau, with only minor drainage development in response to the effects of thrusting Gobi-Altai range to the south, and the Baikal rift basins extending in the north at ~ 7 Ma (San'kov et al., 2000). A complete analysis of the paleo-drainage patterns of the entire Hangay Mountains would be needed to confirm this.

f) From the Miocene to present, the thin Mongolian Plateau maintains a high elevation. This is difficult to reconcile, particularly if the lithosphere is relatively thin here, and more geophysical and geochemical data are needed to speculate further. The compressional and

successor basins of the Valley of Great Lakes were formed to the south of the Hangay Mountains as a product of the Gobi-Altai thrusting (Sladen and Traynor, 2000; Traynor and Sladen, 1995). The Khangai granite was gradually exhumed and formed the resistant low relief range of the Hangay Mountains. The low incision rates measured in this study drive the generation of relief within the range, and are a product of the gradual subsidence of the development of the basins of the Valley of Great Lakes. In summary, it appears that the relief of the western Hangay Mountains, if not the entire Hangay Mountains, is a result of gradual incision of a crustal or lithospheric anomaly that has been essentially geodynamic ally stable for millions of years.

Chapter 6: Conclusions

Landscapes with high elevation and relatively low relief (plateaus) remain a first order problem in intracontinental dynamics. The Hangay Mountains on the Mongolian Plateau in central Mongolia is a large low-relief highland locked in central Asia.

The goal of this study was to determine the cause of relief generation in the western Hangay Mountains. The headwaters of the Dzarvhan River in the western Hangay Mountains have incised into bedrock, and sculpted strath surfaces along the valley. Strath were correlated and dated along the Bogdiin, Chigestei, and Yaruu to create paleo-long profiles. From the strath record, it is apparent that the paleo-long profiles of the streams do not significantly diverge or converge downstream. This suggests that there has not be significant headwater rock uplift or base-level drop since incision of at least half of the valley depth. This is estimated to be on the order of at least a few million years, based on the height of the streams during the last glacial maximum and the cosmogenic nuclide exposure ages on the straths. A slight divergence is apparently favoured by the Yaruu tributary and by the distribution of straths in all three tributaries, which is interpreted to reflect a response to base-level fall associated with subsidence of the Valley of Great Lakes.

More specifically, based on the results in this thesis, the processes governing the relief generation appear to be regional (large scale) as opposed to locally (tectonic-driven) controls on each river. Assuming that the average incision rate has been roughly constant from the period of incision for all three valleys (based on poorly-constrained incision rates of ~0-0.007 mm yr^{-1}), the process driving the incision most likely began before 2.4 Ma. Therefore, the paleo-

long profiles and incision rates imply that the western Hangay Mountains relief is generated from a gradual drop in base-level. This drop in base-level could be accommodated by subsidence of the compression and successor basins forming in the Valley of Great Lakes as a result of thrusting of the Gobi-Altai range.

For future work, the straths along the Chigestei, Bogdiin, and Yaruu that have been observed from digital imagery need to be confirmed from field observations. Future attempts to utilize the strath record should focus on field work necessary to find and use bedload gravels above the straths to help in strath correlation (i.e. on the basis of soil development and sediment provenance). More chronology of the straths is critically needed, and compared to current paleo profile correlation to help constrain the paleo profiles. While a robust comparison with other measures of landscape evolution of the Hangay Mountains (thermo chronology, basin-wide average denudation rates, geomorphometry of the landscape) was beyond the scope of this thesis (in part because that work has not yet been completed or published), it will clearly be necessary to achieve a more complete understanding of the landscape evolution of the Hangay Mountains.

Acknowledgements

A big thank you to my supervisor John Gosse for his patience and support. I would also like to thank Karl Wegmann for this great opportunity for field work in Mongolia. The Mongolia field crew was absolutely amazing, and the work could not have been done without their help every day. This work has resulted from financial support from NSF funding from Dr. Karl Wegmann, and NSERC funding from Dr. John Gosse. Thank you to the Dalhousie Geochronology Center and Guang for processing all of the samples. And lastly, a big thanks to my fellow classmates who were encouraging and helpful.

References

Arzhannikov, S. G., and Arzhannikova, A. V., 2011, The Late Quaternary geodynamics of the Hyargas Nuur basin and bordering scarps (western Mongolia): Russian Geology and Geophysics, v. 52, no. 2, p. 220-229.

Arzhannikova, A. V., and Arzhannikov, S. G., 2008, New data on paleoseismic dislocations in the great lakes basin, western Mongolia: Doklady Earth Sciences, v. 418, no. 1, p. 1-4.

Avouac, J.-P., and Burov, E., 1996, Erosion as a driving mechanism of intracontinental mountain growth: Journal of Geophysical Research, v. 101, no. B8, p. 17747-17717,17769.

Baker, S. E., Gosse, J. C., McDonald, E. V., Evenson, E. B., and Martínez, O., 2009, Quaternary history of the piedmont reach of Río Diamante, Argentina: Journal of South American Earth Sciences, v. 28, no. 1, p. 54-73.

Balco, G., Stone, J. O., Lifton, N. A., and Dunai, T. J., 2008, A complete and easily accessible means of calculating surface exposure ages or erosion rates from< sup> 10</sup> Be and< sup> 26</sup> Al measurements: Quaternary Geochronology, v. 3, no. 3, p. 174-195.

Baljinnyam, I., 1993, Ruptures of major earthquakes and active deformation in Mongolia and its surroundings, Geological Society of Amer.

Barruol, G., Deschamps, A., Déverchère, J., Mordvinova, V. V., Ulziibat, M., Perrot, J., Artemiev, A. A., Dugarmaa, T., and Bokelmann, G. H., 2008, Upper mantle flow beneath and around the Hangay dome, Central Mongolia: Earth and Planetary Science Letters, v. 274, no. 1, p. 221-233.

Barry, T., Saunders, A., Kempton, P., Windley, B., Pringle, M., Dorjnamjaa, D., and Saandar, S., 2003, Petrogenesis of Cenozoic basalts from Mongolia: evidence for the role of asthenospheric versus metasomatized lithospheric mantle sources: Journal of Petrology, v. 44, no. 1, p. 55-91.

Benedict, J. B., 1993, Influence of snow upon rates of granodiorite weathering, Colorado Front Range, USA: Boreas, v. 22, no. 2, p. 87-92.

Bull, W. B., 1990, Stream-terrace genesis: implications for soil development: Geomorphology, v. 3, no. 3, p. 351-367.

Cunningham, D., 2005, Active intracontinental transpressional mountain building in the Mongolian Altai: Defining a new class of orogen: Earth and Planetary Science Letters, v. 240, no. 2, p. 436-444.

Cunningham, W., 2001, Cenozoic normal faulting and regional doming in the southern Hangay region, Central Mongolia: implications for the origin of the Baikal rift province: Tectonophysics, v. 331, no. 4, p. 389-411.

Devyatkin, E., 1974, Structures and formational complexes of the Cenozoic activated stage: Tectonics of the Mongolian People's Republic: Moscow, Nauka, v. 41, p. 182-195.

Donskaya, T. V., Gladkochub, D. P., Mazukabzov, A. M., and Ivanov, A. V., 2013, Late Paleozoic – Mesozoic subduction-related magmatism at the southern margin of the Siberian continent and the 150 million-year history of the Mongol-Okhotsk Ocean: Journal of Asian Earth Sciences, v. 62, no. 0, p. 79-97.

Fifield, L., 1999, Accelerator mass spectrometry and its applications: Reports on Progress in Physics, v. 62, no. 8, p. 1223.

Gosse, J. C., and Phillips, F. M., 2001, Terrestrial in situ cosmogenic nuclides: theory and application: Quaternary Science Reviews, v. 20, no. 14, p. 1475-1560.

Harkins, N., Kirby, E., Heimsath, A., Robinson, R., and Reiser, U., 2007, Transient fluvial incision in the headwaters of the Yellow River, northeastern Tibet: Journal of Geophysical Research, v. 112, p. F03S04.

Jolivet, M., Ritz, J.-F., Vassallo, R., Larroque, C., Braucher, R., Todbileg, M., Chauvet, A., Sue, C., Arnaud, N., and De Vicente, R., 2007, Mongolian summits: An uplifted, flat, old but still preserved erosion surface: Geology, v. 35, no. 10, p. 871-874.

Kovalenko, D. V., 2010, A comparison of Late Mesozoic and Cenozoic intraplate magmatic areas in Central Asia and paleomagnetic reconstructions of the anomalous-mantle location: Russian Geology and Geophysics, v. 51, no. 7, p. 774-784.

Kulakov, I. Y., 2008, Upper mantle structure beneath southern Siberia and Mongolia, from regional seismic tomography: Russian Geology and Geophysics, v. 49, no. 3, p. 187-196.

Lal, D., 1991, Cosmic ray labeling of erosion surfaces:< i> in situ</i> nuclide production rates and erosion models: Earth and Planetary Science Letters, v. 104, no. 2, p. 424-439.

Lambeck, K., Antonioli, F., Purcell, A., and Silenzi, S., 2004, Sea-level change along the Italian coast for the past 10,000 yr: Quaternary Science Reviews, v. 23, no. 14, p. 1567-1598.

Lehmkuhl, F., Klinge, M., and Stauch, G., 2004, The extent of Late Pleistocene glaciations in the Altai and Khangai Mountains: Developments in Quaternary Sciences, v. 2, p. 243-254.

Leland, J., Reid, M., Burbank, D., Finkel, R., and Caffee, M., 1998, Incision and differential bedrock uplift along the Indus River near Nanga Parbat, Pakistan Himalaya, from< sup> 10</sup> Be and< sup> 26</sup> Al exposure age dating of bedrock straths: Earth and Planetary Science Letters, v. 154, no. 1, p. 93-107.

Merritts, D. J., Vincent, K. R., and Wohl, E. E., 1994, Long river profiles, tectonism, and custasy: A guide to interpreting fluvial terraces: JOURNAL OF GEOPHYSICAL RESEARCH-ALL SERIES-, v. 99, p. 14-14.

Montgomery, D. R., 2004, Observations on the role of lithology in strath terrace formation and bedrock channel width: American Journal of Science, v. 304, no. 5, p. 454-476.

Mordvinova, V., Deschamps, A., Dugarmaa, T., Déverchere, J., Ulziibat, M., Sankov, V., Artem'ev, A., and Perrot, J., 2007, Velocity structure of the lithosphere on the 2003 Mongolian-Baikal transect from SV waves: Izvestiya Physics of the Solid Earth, v. 43, no. 2, p. 119-129.

Nishiizumi, K., Imamura, M., Caffee, M. W., Southon, J. R., Finkel, R. C., and McAninch, J., 2007, Absolute calibration of< sup> 10</sup> Be AMS standards: Nuclear Instruments and Methods in Physics Research Section B: Beam Interactions with Materials and Atoms, v. 258, no. 2, p. 403-413.

Pazzaglia, F. J., Gardner, T. W., and Merritts, D. J., 1998, Bedrock fluvial incision and longitudinal profile development over geologic time scales determined by fluvial terraces: GEOPHYSICAL MONOGRAPH-AMERICAN GEOPHYSICAL UNION, v. 107, p. 207-236.

Rizza, M., Ritz, J., Prentice, C., Vassallo, R., Larroque, C., Arzhanikova, A., Arzhanikov, S., Todbileg, M., Javkhlan, J., and Braucher, R., Earthquake geology of the Bulnay Fault, Mongolia, in Proceedings AGU Fall Meeting Abstracts2009, Volume 1, p. 1895.

San'kov, V., Déverchère, J., Gaudemer, Y., Houdry, F., and Filippov, A., 2000, Geometry and rate of faulting in the North Baikal Rift, Siberia: Tectonics, v. 19, no. 4, p. 707-722.

Schumm, S., 1993, River response to baselevel change: implications for sequence stratigraphy: The Journal of Geology, p. 279-294.

Schumm, S. A., 1986, Alluvial river response to active tectonics: Active tectonics, p. 80-94.

Sladen, C., and Traynor, J., 2000, AAPG Studies in Geology# 46, Chapter 2: Lakes During the Evolution of Mongolia.

Stone, J. O., 2000, Air pressure and cosmogenic isotope production: Journal of Geophysical Research, v. 105, no. B10, p. 23753-23723,23759.

Thatcher, W., 2003, GPS constraints on the kinematics of continental deformation: International Geology Review, v. 45, no. 3, p. 191-212.

Traynor, J. J., and Sladen, C., 1995, Tectonic and stratigraphic evolution of the Mongolian People's Republic and its influence on hydrocarbon geology and potential: Marine and Petroleum Geology, v. 12, no. 1, p. 35-52.

Vassallo, R., Jolivet, M., Ritz, J. F., Braucher, R., Larroque, C., Sue, C., Todbileg, M., and Javkhlanbold, D., 2007, Uplift age and rates of the Gurvan Bogd system (Gobi-Altay) by apatite fission track analysis: Earth and Planetary Science Letters, v. 259, no. 3–4, p. 333-346.

Vassallo, R., Ritz, J. F., Braucher, R., Jolivet, M., Carretier, S., Larroque, C., Chauvet, A., Sue, C., Todbileg, M., Bourlès, D., Arzhannikova, A., and Arzhannikov, S., 2007, Transpressional tectonics and stream terraces of the Gobi-Altay, Mongolia: Tectonics, v. 26, no. 5, p. TC5013.

Wakabayashi, J., and Sawyer, T. L., 2001, Stream incision, tectonics, uplift, and evolution of topography of the Sierra Nevada, California: The Journal of Geology, v. 109, no. 5, p. 539-562.

Walker, R., Molor, E., Fox, M., and Bayasgalan, A., 2008, Active tectonics of an apparently aseismic region: distributed active strike-slip faulting in the Hangay Mountains of central Mongolia: Geophysical Journal International, v. 174, no. 3, p. 1121-1137.

Wang, L.-s., Liu, S.-w., Li, C., Li, H., Xu, M.-j., Zhong, K., and Han, Y.-b., 2004, The continental dynamics related to the thermal-rheological structure of the lithosphere: Advance in Earth Sciences, v. 3, p. 005.

Wegmann, K. W., and Pazzaglia, F. J., 2002, Holocene strath terraces, climate change, and active tectonics: The Clearwater River basin, Olympic Peninsula, Washington State: Geological Society of America Bulletin, v. 114, no. 6, p. 731-744.

Wegmann, K. W., and Pazzaglia, F. J., 2009, Late Quaternary fluvial terraces of the Romagna and Marche Apennines, Italy: Climatic, lithologic, and tectonic controls on terrace genesis in an active orogen: Quaternary Science Reviews, v. 28, no. 1–2, p. 137-165.

Yarmolyuk, V., Kovalenko, V., Ivanov, V., and Samoylov, V., 1995, Dynamics and magmatism of late Mesozoic-Cenozoic mantle hot spot, southern Khangai (Mongolia): Geotectonics, v. 28, no. 5, p. 391-407.

Yarmolyuk, V. V., Kovalenko, V. I., Kozakov, I. K., Sal'nikova, E. B., Bibikova, E. V., Kovach, V. P., Kozlovsky, A. M., Kotov, A. B., Lebedev, V. I., Eenjin, G., and Fugzan, M. M., 2008, The age of the Khangai batholith and the problem of batholith formation in Central Asia: Doklady Earth Sciences, v. 423, no. 1, p. 1223-1228.

Yarmolyuk, V. V., Kuzmin, M. I., Vorontsov, A. A., and Khomutova, M. Y., 2013, West Pacific-type convergent boundaries: Role in the crust growth history of the Central-Asian orogen: Journal of Asian Earth Sciences, v. 62, no. 0, p. 67-78.

Appendix

Table A-1. TCN shielding data

MN12-14		MN12-15		MN12-17		MN12-28	
Azimuth (°)	Gradient (°)	Azimuth (°)	Gradient (°)	Azimuth (°)	Gradient (°)	Azimuth (°)	Gradient (°)
45	9	30	8	0	4	21	21
90	23	80	24	33	16	30	21
115	21	105	19	52	25	55	14
130	4	114	5	105	15	80	3
205	8			148	20	110	9
265	16			182	3	210	8
310	8			245	9	230	13
				260	11	255	12
				292	4	268	2
				340	14	336	14

Table A-2. TCN Sample information

Stream Reach	Sample Id	Latitude (°)	Longitude (°)	Lithology	Isotope Targetted
Bogdiin	MN12-14	47.69794	96.97589	Granite	^{10}Be
	MN12-15	47.69688	96.98092	Granite	^{10}Be
Bogdiin Trib	MN12-16	47.60506	97.14900	Granodiorite	^{36}Cl
	MN12-17	47.63228	97.14281	Granite	^{10}Be
	MN12-18	47.63464	97.14483	Granite	^{36}Cl
Chigestei	MN12-09	47.93304	97.02020	Granite	^{10}Be
	MN12-11	47.92451	97.00214	Granite	^{10}Be
	MN12-26	47.84974	96.92940	Granite	^{10}Be
	MN12-27	47.86578	96.93734	Granite	^{10}Be
Chigestei Trib	MN12-28	47.92894	97.14264	Granite	^{10}Be
Yaruu	MN12-12	48.06650	96.72267	Gabbro	^{36}Cl
	MN12-13	48.06677	96.72242	Gabbro	^{36}Cl

Table A-3. Reduced Chemical Data

Field ID	Lab ID	Qtz Mass (g)	Carrier Mass (g)	Carrier ID (txt)	Carrier Conc (mg/mL)	Carrier Density (g/mL)	^{9}Be added (atoms 9Be)	Blank ID (txt)	Chemistry Comment
MN12-09	JG2823	25.0221	0.9003	BeCarrier31-2012-bot1	275	1.013	1.633E+19	2814	Normal
MN12-11	JG2824	25.1974	0.8985	BeCarrier31-2012-bot1	275	1.013	1.630E+19	2814	Normal
MN12-14	JG2825	25.0914	0.9102	BeCarrier31-2012-bot1	275	1.013	1.651E+19	2814	Normal
MN12-15	JG2826	20.0292	0.9010	BeCarrier31-2012-bot1	275	1.013	1.634E+19	2814	Normal
MN12-17	JG2828	24.8910	0.8984	BeCarrier31-2012-bot1	275	1.013	1.630E+19	2814	Controlled PP, 17ml Cation, then 2ml Cation, large Al gel
MN12-26	JG2830	20.0035	0.8980	BeCarrier31-2012-bot1	275	1.013	1.629E+19	2814	*After 1st Be(OH)2, large size Gel, re-do 2ml Cation, Ti removal
MN12-27	JG2831	20.0207	0.8912	BeCarrier31-2012-bot1	275	1.013	1.617E+19	2814	*After 1st Be(OH)2, large size Gel, re-do 2ml Cation, Ti removal
MN12-28	JG2832	20.0213	0.9016	BeCarrier31-2012-bot1	275	1.013	1.636E+19	2814	Normal

Table A-4. AMS measured normalized data

Field ID	Lab ID	LLNL ID	# Runs	True Frac	Normalized $^{10}Be/^{9}Be$ Measured	1σ Unc	Precision 1σ (%)	AMS Comment
MN12-09	JG2823	BE34487	4	0.9946	high boron: LvFr <0.85			v high B
MN12-11	JG2824	BE34488	3	0.9933	high boron: LvFr <0.85			V V high B
MN12-14	JG2825	BE34489	3	0.9991	4.952E-12	6.127E-14	1%	high B
MN12-15	JG2826	BE34490	3	0.9988	3.007E-12	3.991E-14	1%	high B
MN12-17	JG2828	BE34491	4	0.9995	1.620E-12	2.855E-14	2%	ok B
MN12-26	JG2830	BE34492	3	0.9979	1.054E-12	1.953E-14	2%	ok B
MN12-27	JG2831	BE34493	3	0.9999	3.475E-12	7.069E-14	2%	ok B
MN12-28	JG2832	BE34494	3	0.9981	2.657E-12	6.902E-14	3%	high B low current

Table A-4. AMS measured normalized data

	$^{10}Be/^{9}Be$ AMS boroncorr ($^{10}Be/^{9}Be$)	1σ Error ($^{10}Be/^{9}Be$)	(%)	^{10}Be atoms (atoms)	^{10}Be atoms total error (atoms)	^{10}Be atoms blank corr (atoms)
MN12-09	*n.d.*					
MN12-11	*n.d.*					
MN12-14	4.952E-12	6.127E-14	1.2%	8.176E+07	8.172E+07	1.922E+06
MN12-15	3.007E-12	3.991E-14	1.3%	4.914E+07	4.910E+07	1.179E+06
MN12-17	1.620E-12	2.855E-14	1.8%	2.639E+07	2.636E+07	7.027E+05
MN12-26	1.054E-12	1.953E-14	1.9%	1.716E+07	1.712E+07	4.669E+05
MN12-27	3.475E-12	7.069E-14	2.0%	5.617E+07	5.613E+07	1.601E+06
MN12-28	2.657E-12	6.902E-14	2.6%	4.346E+07	4.342E+07	1.423E+06

Notes:

Blank was 7e-15, however it had very high boron and large uncertainty. Used average of two other blanks analysed in same run

Average blank ratio was 2.4E-15, or 3.918 x 10^{4} atoms of ^{10}Be